People's Democratic Republic of Algeria
Ministry of Higher Education and Scientific Research
University of Médéa
Faculty of Science

Thesis

Presented to the department of Matter Science
to obtain the degree of

Master of Physics

Discipline: material physics

By:
Romaissa Kali

Theme:

Structural Electronic and Magnetic Characterisation of Mn_2FeSn Heusler Alloy .

10 September 2021

Jury members:

Dr. Abdelali Boukaoud	MCA	University of Medea	President
Dr. H. Lachenani	MCB	University of Medea	Examiner
Dr. Djamel Sebbar	MCB	University of Medea	Examiner
Dr. Mourad Dehbaoui	MCA	University of Medea	Supervisor

Academic year 2020/2021

abstract

In this master thesis, we present the first-principle calculations of the structural, electronic and magnetic properties of the inverse Heusler compound Mn_2FeSn with discussions in order to identify the characteristics in the interest of spintronics devices.

To determine its properties, we carried out a theoretical study using the pseudo-potential approximation coupled to the plane wave (PP-PW) within the framework of the density functional theory (DFT) implemented in CASTEP.

The exchange-correlation potential was treated by generalized gradient approximation (GGA) according to Perdew, Burke and Ernzerhof (PBEsol).

We performed a geometric optimization under stress between -12 and 12 GPa for the three predicted structures of the compound in order to obtain the most stable.

At equilibrium state, we have discovered that the compound Mn_2FeSn behaves like a half-metal semiconductor, metal and a gapless half-metal, according to the different values of the pressure imposed.

The total and partial density of state indicates a polarization ratio equal to (57%) calculated at the Fermi level. The found value of the magnetic moment of 2 μB agrees with the Slatter-Pauling rule.

The subject compound of our study exhibits a great diversity of behaviour under hydrostatic pressure. Which makes him a promoter candidate for the next generation of spintronic applications and nanoelectronic devices.

Keywords: spintronic, Mn_2FeSn, inverse Heusler, GGA PBEsol, Half metallic.

ملخص

في أطروحة الماستر هذه ، نقدم حسابات المبدأ الأول للخصائص الهيكلية، الإلكترونية والمغناطيسية للمركب العكسي Heusler Mn_2FeSn مع مناقشات لاستنتاج مميزات لصالح أجهزة spintronics .

من أجل تحديد خصائصه، أجرينا دراسة نظرية اعتمادا على تقريب شبه الكمونات المقترنة بالموجة المستوية (PP-PW) في إطار نظرية دالية الكثافة الالكترونية أ (DFT) المطبقة في برنامج (CASTEP) .

تمت معالجة إمكانات الارتباط التبادلي عن طريق تقريب التدرج المعمم (GGA) وفقًا لـ Perdew و Burke و Ernzerhof (PBEsol) .

أجرينا تحسينًا هندسيًا تحت الضغط يتراوح بين 12- و 12 GPa للهياكل الثلاثة المتوقعة للمركب من أجل الحصول على الأكثر استقرارًا.

في حالة التوازن، اكتشفنا أن المركب Mn_2FeSn يتصرف مثل نصف معدني شبه موصل، معدن و نصف معدن بلا فجوة، وفقًا للقيم المختلفة للضغط المطبق.

تشير الكثافة الكلية والجزئية للحالة إلى نسبة استقطاب تساوي (57%) محسوبة على مستوى $Fermi$.

تتوافق القيمة التي تم العثور عليها للعزم المغناطيسي البالغ μB 2 مع قاعدة Slatter-Pauling .

يُظهر المركب موضوع دراستنا تنوعًا كبيرًا في السلوك تحت الضغط الهيدروستاتيكي. مما يجعله مرشحًا ممتاز للجيل القادم من تطبيقات spintronics والأجهزة الإلكترونية النانوية.

الكلمات المفتاحية: انصاف المعادن، spintronic ، Mn_2FeSn ، معكوس Heusler ، GGA PBEsol .

Résumé

Dans ce mémoire de master, nous présentons les calculs de premier principe des propriétés structurales, électroniques et magnétiques du composé inverse Heusler Mn_2FeSn avec des discussions dans le but d'identifier les caractéristiques dans l'intérêt des dispositifs de spintronique.

Pour déterminer ses propriétés, nous avons réalisé un calcul ab initio utilisant les approximations des pseudo-potentiels (PP) et des ondes planes (PW) dans le cadre de la théorie de la fonctionnelle de la densité (DFT) implémentée dans CASTEP.

Le potentiel d'échange-corrélation a été traité par l'approximation du gradient généralisé (GGA) selon Perdew, Burke et Ernzerhof (PBEsol).

Nous avons fait une optimisation géométrique sous contrainte entre -12 et 12 GPa pour les trois structures prédites du composé afin d'obtenir la plus stable.

À l'état d'équilibre, nous avons découvert que le composé Mn_2FeSn se comporte comme un semi-conducteur demi-métallique, comme un métal et comme un gapless demi-métal, selon les différentes valeurs de la pression imposées.

La densité d'état totale et partielle indique un rapport de polarisation égale à (57%) calculé au niveau de Fermi. La valeur trouvée du moment magnétique de 2 μB est en accord avec la règle de Slatter-Pauling.

Le composé sujet de notre étude, présente une grande diversité de comportements sous pression hydrostatique. Ce qui fait de lui un candidat promoteur pour la prochaine génération d'applications spintroniques et des dispositifs nanoélectroniques.

Mots clés : spintronic, Mn_2FeSn, inverse Heusler, GGA PBEsol, Demi Métallique.

إهداء

لله الحمد والشكر والفضل والثناء الحسن
فلولاه لما وفقنا لما نحن عليه
اهدي مذكرة تخرجي الى والداي اللذان لهما الفضل الكبير بعد الله عز و جل فلولا فضلهما وسعة صبرهما علي لما كنت هنا
حفظهما الله لى وبارك لي فيهما وأطال عمرهما بالصحة والعافية
الى زوجي وأطفالي وأختي خولة وكل عائلتي الكريمة
الى اساتذتي الكرام خلال مشواري الدراسي كله
الى كل صديقاتي العزيزات
واخيرا الى كل من كان له فضل علي ولو بكلمة طيبة
داعية المولى عز وجل ان يحفظكم وأهليكم من كل سوء

كالي رميصة

Acknowledgements

First, I thank God for giving me health, wellness and determination during my years of study to completion of this work.

I would like to extend my special thanks to everyone who helped me and everyone who has supported me from near or far to complete my study journey.

I would like to thanks and honour my teachers for guiding us, teaching us and the knowledge they provided us during these years at Dr Yahya Fares University in Medea.

I especially thank my supervisor, Dr Debhaoui, for his advice and support with his valuable guidance and efforts throughout the thesis work.

I also extend my sincere thanks to Dr Lachnani, Dr Houatis, Dr Houhou, my dear friend Mrs Ilham and all the teacher's who overseeing us during this year, and it was an honour for me to attend their valuable classes.

I also express my gratitude to all the people and assistants in the lab especially Mrs Khadija for her kindness and availability.

Finally, this thanks would not be complete without mentioning the merit of my family and friends for their encouragement and support that allowed me to conclude this work in the appropriate circumstances.

Contents

List of Figures xi

General introduction xii

Notation and abbreviations xiv

1 Magnetism and spintronics 1
- 1.1 Introduction . . . 1
- 1.2 Magnetism on Microscopic Scale . . . 1
- 1.3 Types of magnetic arrangement . . . 2
  - 1.3.1 Diamagnetism . . . 2
  - 1.3.2 Paramagnetism . . . 4
  - 1.3.3 Ferromagnetism . . . 4
  - 1.3.4 Antiferromagnetism . . . 6
  - 1.3.5 Ferrimagnetism . . . 7
- 1.4 Macroscopic magnetism . . . 8
  - 1.4.1 Hysteresis cycle . . . 8
- 1.5 Magnetic anisotropy . . . 9
  - 1.5.1 Magnetocrystalline anisotropy . . . 9
  - 1.5.2 Shape anisotropy . . . 10
- 1.6 Spintronic Devices and Magnetoresistance . . . 11
  - 1.6.1 Giant magnetoresistance (GMR) . . . 11
  - 1.6.2 Tunnel magnetoresistance (TMR) . . . 12

2 Heusler alloy 13
- 2.1 Introduction . . . 13
- 2.2 Crystal Structure of Heusler Compounds . . . 15
- 2.3 Half-metallic ferromagnet . . . 15
- 2.4 Spin gapless semiconductor . . . 17
- 2.5 Origin of the Gap . . . 19

2.6 The Slater-Pauling rule . . . 21

3 Foundations of the density functional theory **24**
3.1 Introduction . . . 24
3.2 Schrödinger equation . . . 25
3.2.1 Born Oppenheimer approximation . . . 26
3.3 Density functional theory . . . 26
3.4 Hohenberg and Kohn's theorem . . . 27
3.4.1 First Hohenberg-Kohn Theorem . . . 27
3.4.2 Second Hohenberg-Kohn Theorem . . . 28
3.5 Kohn and Sham theorem . . . 28
3.6 Exchange-correlation approximations . . . 30
3.6.1 The Local density approximation (LDA) . . . 31
3.6.2 Generalized gradient approximation (GGA) . . . 31
3.6.3 PBEsol exchange-correlation functional from Perdew–Burke– Ernzerhof approximation (GGA) . . . 32
3.7 Solving the Kohn-Sham equations . . . 32
3.8 Bloch's theorem and plane wave basis set . . . 34
3.9 pseudos-potentials Method . . . 35

4 Results and discussions **38**
4.1 Calculation parameters . . . 38
4.2 Structural properties of compounds . . . 39
4.2.1 Crystal structure . . . 39
4.2.2 Equilibrium state and Pressure effect . . . 42
4.3 Electronic properties of compounds . . . 44
4.3.1 Brillouin zone . . . 44
4.3.2 Band structure . . . 45
4.3.3 pressure effect on the energy gap . . . 49
4.3.4 Densities of states (TDOS,PDOS) . . . 50
4.4 Magnetic properties of compounds . . . 50
4.4.1 Magnetic moment . . . 50
4.4.2 Pressure effect on Magnetic moment . . . 52
4.4.3 Spin polarization . . . 52

Conclusion **55**

A Fundamental notions associated with the CASTEP code use **57**
A.1 The CASTEP code . . . 57
A.2 Geometric optimization . . . 58
A.3 Electronic band structure . . . 58
A.4 Density of state . . . 59

A.5 The atomic population of Mulliken 59

List of Figures

1.1 Schematic diagram of magnetization of diamagnetic materials, with a negative magnetic susceptibility and a permeability of slightly less than that of vacuum[1] 3
1.2 Typical behavior of diamagnetic and paramagnetic materials depending on an external magnetic field and temperature[2] 3
1.3 Schematic diagram of magnetization of paramagnetic materials, with low values of susceptibility and permeability[1]. . . . 5
1.4 Domain formation in a ferromagnetic sample (a) without field, (b) with some field applied, (c) with a strong linear field, and (d) a closer look at the domain wall formation[2]. . . . 5
1.5 Schematic diagram of spin-ordering in antiferromagnetic materials 7
1.6 Schematic diagram of spin-ordering in ferrimagnetic materials 7
1.7 Magnetic hysteresis in a ferromagnetic material. Intercepts points H_C and M_R are the coercivity and the remanence respectively 9
1.8 Surface magnetic pole and internal demagnetizing field H_d (dashed arrow) for an ellipsoidal grain with uniform axial magnetization M[3]. . . . 10

2.1 Periodic table of the elements. The huge number of Heusler materials can be formed by combination of the different elements according to the color scheme[4] 14
2.2 Schematic representation of the various structures of the semi- and full-Heusler compounds.[5] 14
2.3 Different types of Heusler structures. Full-Heusler (a), Half-Heusler (b),Inverse-Heusler (c), and Quaternary-Heusler structures (d)[6]. . . . 16
2.4 Inverse and regular structure for Mn2-based Heusler compounds[6, 7]. . . . 16
2.5 The electronic band structures of various classes of materials, metal, semiconductor, half and semi metal[8]. . . . 17
2.6 The schematic density of states n(E) as a function of energy E is shown for (a) a half-metallic ferromagnet, (b) a spin gapless semiconductor,, and (c) a zero-gap half-metallic ferromagnet. The occupied states are indicated by filled areas. Arrows indicate the majority (↑) and minority (↓) states[9]. . . . 18

2.7 Energy band diagrams for spin gapless semiconductors with parabolic dispersion between energy and momentum[8]. 18
2.8 Schematic illustration of the origin of the gap in the minority band in inverse-Heusler alloys Mn_2FeSn. The dashed line represents the location of the Fermi level E_F[10, 11]. 20
2.9 The values for 3d transition metals and their alloys are given for comparison[4]. . . 21
2.10 Calculated total spin moments for all the studied full Heusler alloys. The dashed line represents the Slater-Pauling behaviour[12]. 22
2.11 Calculated total spin moments for several inverse Heusler compounds studied.The dashed lines represent the three variants of the Slater-Pauling behaviour for these compound[12]. 22

3.1 Diagram illustrating the concept of interactive real system and the non-interactive fictitious system ; (a): Real system made up of several electrons in mutual interaction; (b): fictitious system of independent fermions with the same energy and the same electron density as the real system[13, 14]. 29
3.2 Schematic representation of the self-coherent cycle within the framework of the Functional Theory of Density. The electron density constitutes the fundamental quantity which governs the iterative procedure by defining both the starting point and the end point of the self-coherent cycle[15]. 33
3.3 Schematic illustration of all-electron (solid lines) and pseudo electron (dashed lines) potentials and their corresponding wave functions[16]. The radius at which all-electron and pseudo electron values match is designated r_c. 37

4.1 different site occupations for the three types with atoms on Wycoft position [4] . . . 40
4.2 Schematic represent lattice parameter experimental and theoretical, the final minimum energies values for the three different configurations for the primitive and conventional cell 40
4.3 Schematic representation of Mn_2FeSn inverse Heusler site occupancies structures . 40
4.4 Schematic representation of Mn_2FeSn inverse Heusler primitive cell.the preferred occupations for the different lattice sites are 4c (1/4,1/4,1/4), and 4d (3/4, 3/4, 3/4) for the double Mn ,and 4a (0,0,0), 4b (1/2,1/2,1/2) for Sn and Fe respectively 41
4.5 Schematic represent the variation of the total energy as a function of the pressure applied and the volume for the three different configurations for the conventional cell. 41
4.6 Total energy evolution as a function of the volume for the primitive and conventional cells 43
4.7 Quantities values that obtained in the equilibrium state 43
4.8 Pressure effect on lattice parameter and cell volume for the primitive cell 44
4.9 The first Brillouin zone for the Mn_2FeSn FCC lattice.g 1, g 2, g 3 are the reciprocal base vectors 45
4.10 Schematic representation the band structures of 0 and -4 GPa for majority and minority spin. 46

4.11 Schematic representation of the band structure for minority spin under different pressure(0, 2, 4, 8, 12, -1 GPa). 47
4.12 Schematic representation of the band structure for minority spin under different pressure (-2, -4, -8, -12 GPa). 48
4.13 Pressure effect on the forbidden band 49
4.14 Calculated spin-projected total and partial DOS plots for Mn_2FeSn at 0 GPa. . . . 51
4.15 Total and partial magnetic moment as a function of pressure. 52
4.16 Calculated spin-projected total DOS at 0 GPa for the inverse Heusler Mn_2FeSn. . 53
4.17 Calculated spin-projected total DOS Mn_2FeSn[17]. 54
4.18 Percentage polarization values versus pressure. 54

General introduction

It was difficult to understand physics of electrons in solids before modern physics, and this was the key feature of condensed matter physics or physics of matter, which is today occupy 50% of different research domains in physics sciences. From best known applications, spintronic and information processing (semiconductors, magnetic data storage), communications, and medical imaging (superconductivity and magnetism).

The discovery of Giant Magnetoresistance (GMR) in 1988 laid the foundation to an entirely new research field under the name Spin-electronics or Spintronics, it exploit the electron spin and electron charge currents and opened the door to a new generation of high speed, low power in electronic devices.

The success of spintronics relies on the ability to create, control, manipulate and detect spin orientation and coherence over practical time and length scales[18, 19, 20, 21, 22, 23, 24].

Recently, Heusler compounds have attracted great attention due to their magnetic behaviour, in addition, these types of materials provide novel features in spintronic microelectronics and magneto-electronic devices[23, 25].

In Heusler compounds, both spin directions display atypical behaviour at the Fermi level: one spin direction exhibits a metallic behaviour, whereas the other spin shows a semiconducting character which leads to a 100% spin polarization at the Fermi level. In ferromagnetic compounds, the hybridization between metal and semiconductors is called half metallic (HM), which is the character of several Heusler alloys that was investigated theoretically as well as most magnetic properties, through the first principle ab initio methods[26, 27, 5, 4].

G. H. Wen and X. X. Zhang, successfully synthesized the magnetic shape memory alloys, of the novel ferromagnetic Heusler Mn_2FeSn considering it as a metastable modulated martensite that can generate a switching-like giant strain as shown in $Ni_{52}Mn_{24.5}Ga_{23.5}$[28] study[29, 30].

This compound exhibits a Ferromagnetic shape memory alloys effect which have become one of the significant subjects in materials science and condensed matter physics fields, and renders it an excellent candidate for potential applications as magnetic field controlled actuators that have a big importance in electronics material, transducers, sensors, aerospace, and military fields because of their high response frequency[25, 31, 23, 30].

Several methods have been developed to predict the physical and chemical properties of solid materials and preparing for applied experiments, which can be classified into two categories, quasi-

experimental and ab initio methods[32, 30].

Based on quantum mechanics principles, and according to the interaction between the nucleus and electron systems correlation such as those in molecules, and other condensed matter systems, the first principles method finds the solution to the Schrödinger equation through series of approximations and simplifications to deal with the N-body problem. Among these methods, the modelling method density functional theory (DFT).

The waves function describes these systems that totally specify the state of electrons and therefore depend not only on the coordinates of electrons but also on their spins. Applying this process requires an analysis of the invariant Schrödinger equation which depends on 3N spatial and spin-N variables.

Ab initio (from first principles) DFT calculations permit the prediction and calculation of material behaviour. In modern DFT techniques the electronic structure is evaluated using a potential acting on the system's electrons.

In DFT his based on considering that the total energy of the system is a function of the electronic density, which is itself a function of the space coordinates[33, 34, 35, 36, 37].

The principal aim of this master's thesis is to understand the basic properties of the Mn2FeSn Heusler compound.

- In the first chapter 1, some concepts related to magnetism and its types were presented, and some applications related to ferromagnetic compounds in technology such as GMR and TMR.
- In the second chapter 2, we presented Heusler alloys with their different types and physical properties.
- In the third chapter 3, we explained the basis of the density functional theory (DFT), besides the different approximations, the pseudo-potential and plana wave (PP-PW) method that it used in this simulation.
- The fourth chapter 4 is devoted to the study the compound properties with a discussion of calculations details structural, electronic (band structure, gap, state density) and magnetic properties (magnetic moment, polarization), implemented in the CASTEP software code[33].

Finally, we end our work with a general conclusion summarizing the work and results.

Notation and abbreviations

Abbreviations

DFT : Density Functional Theory
NMR : Nuclear magnetic resonance
IT : Information technology
MR : Magnetoresistive
GMR : Giant magnetoresistance
TMR : Tunnelling magnetoresistance
MRAM : Magnetic random access memory
DMS :diluted magnetic semiconductors
CIP : Schematic diagram of current in the plane
CPP : current perpendicular to the plane GMR stack
LDA : Local density approximation
GGA : gradin generalized approximation
PBE :Perdew-Burke-Ernzerh
EXC : Exchange-Correlation energy
PBEsol :Perdew-Burke-Ernzerh for solid
CASTEP : Cambridge Serial Total Energy Package
PP : pseudo potential
PW : plane wave
EOS : Equation of state
B_0 : Bulk modulus
B' : Derived from the pressure of the compressibility modulus
E_F : Fermi energy
E_g : Band gap (Energy band gap)
TDOS : total density of state
PDOS : partial density of state
fcc : face-centered cubics
hcp : hexagonal closed packed
bcc : body-centered cubic

MBE : molecular beam epitaxy
HDD : hard disk drive
HMF : half-metallic ferromagnet
FM : ferromagnet
NM : non-magnet
LCAO : linear combination of atomic orbitals
MO : molecular orbital
SCF : Self-Consistent Field
BFGS : Broyden-Fletcher-Goldfarb-Shanno (algorithm)
BZ : Brillouin zone

Notations

H : Champ magnetic.
M : Aimantation.
B : Induction magnetic.
χ : Susceptibilite magnetic.
μ : Permeabilite magnetic.

Chapter 1

Magnetism and spintronics

1.1 Introduction

Spintronics is a new field of science, developed over the past 20 years, that is focused on exploring the properties of materials in which spin-polarized currents play a key role, as well as developing materials and devices for advanced nano-electronic applications [18].

For realizing various spintronic devices, materials with strong spin polarization are the key, such as ferromagnetic and half-metallic materials. To date, various half-metallic materials studied theoretically and experimentally, such as Perovskite, Spinel, zinc blend structure, Heusler alloys, etc Amongst the expected advantages of spintronics technologies, researchers have identified the non-volatile storage of data with high density and low energy consumption[38]. Spintronics materials have already found one important application as highly sensitive magnetic field sensors in recording read heads for magnetic disk drives, Their development based on the discovery of giant magnetoresistance (GMR) and oscillatory inter-layer magnetic coupling in magnetic multi-layers in the early years1990[39, 40] .

1.2 Magnetism on Microscopic Scale

If we continue to cut a permanent magnet, we would get to the atomic scale. The question is: which elementary particles handle magnetic behavior.

We shall show that elementary magnetic dipole moment is proportional to the specific charge so electrons handle the dominant magnetic properties. Electrons can generate magnetism in three ways:

- As moving charges as current
- Because of their spin
- Because of their orbital rotation around a nucleus

That two mechanisms add together to handle magnetic behavior in particular materials. ms-mb is called Bohr magneton and it is the smallest magnetic dipole moment that can exist in Nature. So it serves as a microscopic unit for dipole moments.When electrons are bound in atoms they also have orbital angular momentum. It is illustrative to look at a classical planetary model of the electron,even if it is not realistic, to see where the dependence on the specific charge comes from. Even in a very small but macroscopic piece of material there is an enormous number of electrons, each having some spin and some angular momentum. The total internal magnetic field is a superposition of all-electron dipole moments [41, 42].

1.3 Types of magnetic arrangement

In the free state, an atom is magnetic if it carries a permanent magnetic moment represented by a vector of constant modulus. All materials are made up of a set of atoms which can be magnetic or non-magnetic. With the magnetic assembly, the direction and sometimes the modulus of the magnetic moments can depend on the particular environment of each atom (nature and position of neighboring atoms, temperature and applied magnetic field)[43].These magnetic moments can align by applying a magnetic field that produces proportional magnetization M at induction field H.[44].

$$\vec{M} = \chi \vec{H} \ . \tag{1.1}$$

Everything has magnetic properties, so it is not surprising that magnetism can be used for both quantitative and qualitative analysis. Magnetism can be used for bulk analysis, distinguishing particular elements especially different metals in compounds, and for indicating structure types. Magnetic properties are best used in conjunction with other properties, and the more is known about a sample, the more use can be made of the magnetic properties [45, 26].There are different types of magnetism.

1.3.1 Diamagnetism

Diamagnetism characterizes substances that have only non-magnetic atoms: their magnetization[43], originates from the change in the electronic orbital motion under the effect of the applied magnetic field, is very weak, and thus the magnetization (M), which is in the opposite direction to that of the external magnetic field, as schematically shown in Fig 1.1. This magnetism also exists in substances with magnetic atoms, but it is so weak that it is then completely masked by the contribution of these magnetic atoms[1]. According to the Lenz law, the induced currents give rise to an induction flux opposite to the change in the applied field shown in Fig 1.2.

The diamagnetism susceptibility,virtually independent of the field and temperature, is negative.

$$\chi^{dia} = \text{const} < 0 \ . \tag{1.2}$$

A few examples of diamagnetic materials are:

- Nearly all organic substances,

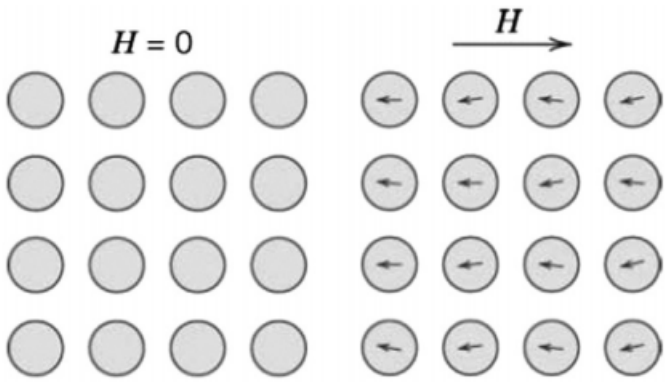


Figure 1.1: Schematic diagram of magnetization of diamagnetic materials, with a negative magnetic susceptibility and a permeability of slightly less than that of vacuum[1]

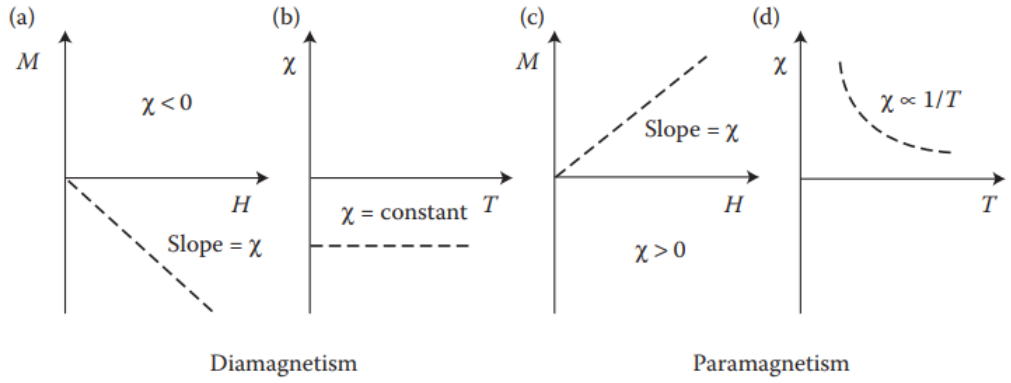


Figure 1.2: Typical behavior of diamagnetic and paramagnetic materials depending on an external magnetic field and temperature[2]

- Metals like Hg or noble metals like Cu,
- very strong diamagnetism present in superconducting substances under critical temperature , with a susceptibility equal to -1.These materials are ideal diamagnets[46].

Applied magnetic fields induce currents in electric conductors, and this includes electron orbits and the induced currents in turn decrease magnetic field strength within the conductors.These are the shielding currents that are the basis of nuclear magnetic resonance(NMR) spectroscopy[45, 2].

1.3.2 Paramagnetism

Electrons and nucleons have angular momentum (and hence the magnetism of a moving charge) as if they had a spin and orbital motion[45]. Paramagnetism is because of unpaired spins. It is a type of magnetism where there are no interactions between magnetic moments[46].

A paramagnetic substance is any substance that contains magnetic atoms whose moments disordered in all directions because of their thermal agitation by definition, all materials that are not diamagnetic are paramagnetic[44], the individual magnetic moments do not interact magnetically, and like diamagnetism, the magnetization is zero when the field removed.

In the presence of a field(see Fig 1.3, there is now a partial alignment of the atomic magnetic moments in the field's direction, resulting in a net positive magnetization and positive susceptibility $\chi > 0$ see Fig 1.2.

At high values of magnetization fields, all the magnetic moments are parallel to each other, and the magnetization reaches its maximum value (saturation MS)[47, 2, 1]. For a certain value of the applied magnetic field, after decreasing temperature, this relative orientation of the magnetization and, at 0 K, the magnetization reaches its maximum value.The magnetic susceptibility, obtained for low values of the applied magnetic field, is given by Curie law:

$$\chi^{para} = \frac{C}{T} \ , \tag{1.3}$$

where C is the Curie constant.

1.3.3 Ferromagnetism

Ferromagnetic materials are strongly magnetized toward the applied magnetic field. It possesses an enormous permanent magnetic moment in each atom. It follows an alignment of the magnetic moments on the microscopic scale and the appearance of a microscopic spontaneous magnetization without an applied magnetic field.

The presence of permanent magnetic moments in the atoms or molecules in the specimen gives rise to ferromagnetism as this magnetic moment aligns itself in the same direction as that of the external field, that external magnetic field produces an extensive amount of induced magnetic moment which increases the magnetic induction present in the specimen[48].

In a ferromagnetic material, three types of interactions coexist exchange interactions, interactions with the lattice, and magnetic dipole interactions[49]. The exchange interaction between

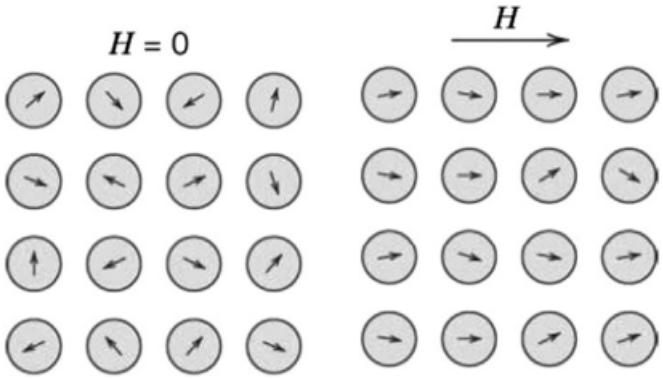


Figure 1.3: Schematic diagram of magnetization of paramagnetic materials, with low values of susceptibility and permeability[1].

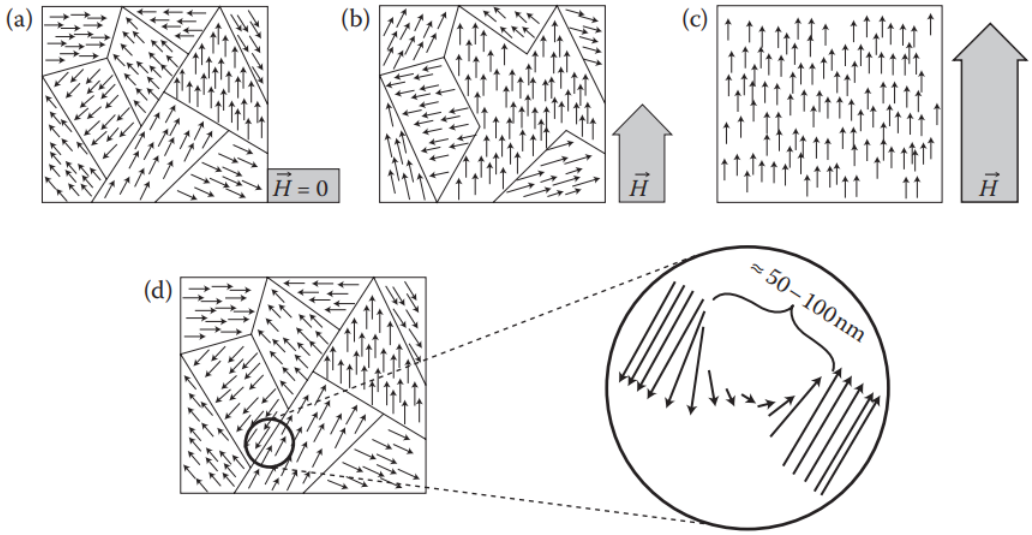


Figure 1.4: Domain formation in a ferromagnetic sample (a) without field, (b) with some field applied, (c) with a strong linear field, and (d) a closer look at the domain wall formation[2].

unpaired electrons of adjacent atoms in the crystal lattice gives rise to a local molecular magnetic field resulting in spontaneous magnetization[44].

Exchange forces are very large, equivalent to a field on the order of 1000 Tesla. The exchange force is a quantum mechanical phenomenon due to the relative orientation of the spins of the two-electron[47]. the magnetic phenomenon of the positive exchange interaction between neighboring moments causes the alignment of magnetic moments in parallel arrangement to each other which results in a large net magnetization even in the absence of a magnetic field (see the Fig 1.4).At relatively high temperatures, thermal agitation leads to a susceptibility similar to that of a paramagnetic substance: this is the Curie-Weiss law

$$\chi = \frac{C}{T - T_C} \ . \tag{1.4}$$

However, the magnetic susceptibility instead of being infinite at 0 Kelvin as in a paramagnetic substance becomes infinite at the Curie temperature T_C and this is due to the existence of magnetic interactions.Below this temperature, thermal agitation is dominated by magnetic interactions and spontaneous magnetization M_S occurs in the absence of an applied field [50, 2].

1.3.4 Antiferromagnetism

Antiferromagnetism is a cooperative ordering that can be understood by considering two magnetic sub-lattices: M_A and M_B , of the same magnitude (see Fig 1.5. Each one is ferromagnetic and behaves (approximately), according to the description mentioned above. The difference is that both sub-lattices oriented in opposition,the total magnetization vanishes [46].

$$M = M_A + M_B = 0 \ . \tag{1.5}$$

Unlike ferromagnetic substances, an antiferromagnetic material has a weak magnetism similar to paramagnetism in that the susceptibility is low and positive. Generally, antiferromagnetic order may exist at sufficiently low temperatures, vanishing at and above a certain temperature, the transition temperature called Neel temperature(named after Louis Neel, who had first identified this type of magnetic ordering)[48].

Above the Neel temperature, the material is typically paramagnetic.hence, the thermal variation of the inverse of the susceptibility, measured on a polycrystalline substance, finds its minimum at Neel temperature.Neel's law gives the expression of the magnetic susceptibility of antiferromagnetic compounds:

$$\chi = \frac{C}{T + T_N} \ , \tag{1.6}$$

When the temperature increases the magnetic susceptibility decreases to the temperature of Neel T_N .For $T > T_N$,the compound becomes paramagnetic[44].

This antiparallel arrangement of the spins results from interactions between neighbouring atoms (called negative exchange interactions).These oppose the action of the applied magnetic field which reinforces the parallelism of the individual magnetic moments[50, 2].

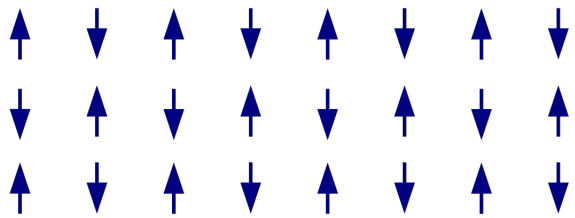


Figure 1.5: Schematic diagram of spin-ordering in antiferromagnetic materials

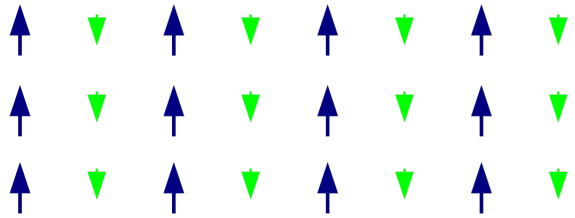


Figure 1.6: Schematic diagram of spin-ordering in ferrimagnetic materials

1.3.5 Ferrimagnetism

In ferrimagnets material, the magnetic moments of the A and B sub-lattices are not equal don't have the same magnetization (see Fig 1.6, and result in a net magnetic moment. Ferrimagnetism had been observed in compounds with more complex crystal structures than single elements.

$$M_a \neq M_b \ . \tag{1.7}$$

In the ferrimagnetic there is an equal number of crystal sub-lattices from opposite directions but the magnetic alignment of one subset may be stronger than the other. The number of crystal sub-lattices in one direction is greater than the number in the other direction[44]. The spin moments of atoms can be opposite; the resulting moment being positive,or negative[50].

$$M = M_a + M_b \neq 0 \ . \tag{1.8}$$

Therefore Ferrimagnetism is like ferromagnetism. It exhibits all the characteristics of ferromagnetic behaviour spontaneous magnetization, Curie temperatures, hysteresis, and remanence[47].in addition to the high resistivity and anisotropic properties.An external applied field induced the anisotropy. However, ferro- and ferrimagnets have very different magnetic ordering[48].

Finally, Ferrimagnetism disappears if we overstep a certain temperature, called the Curie temperature. the magnetic susceptibility only follows the Curie-Weiss law for a very high temperature[46, 2].

1.4 Macroscopic magnetism

The origin of the macroscopic magnetism in solids is the atomic magnetic moment and the mutual coupling of their individual atoms (and which originates from the spin and angular momenta of the electron)[51].

The fundamental wonder is how this microscopic magnetism gives rise to the macroscopic magnetism of solids appearing in some materials below the transition temperature, called Curie temperature, T_C.

There are two main and opposite streams: localized and itinerant magnetism models. The former models start with the electronic states localized in real space, which considers that the electrons responsible for the magnetism remain localized surrounding their nuclei,examples of these are Heusler alloys, metallic gadolinium, and, in particular, the transition metal monoxides[52].The simplest magnetic exchange mechanisms are ones, where the electrons can be looked at as being localised[53].

while the latter(itinerant magnetism) starts with those states localized in reciprocal space, which also considers that the responsible conduction electrons for the magnetism are dislocated and totally free to move in any space in the tire of the material[54].

1.4.1 Hysteresis cycle

The most usual manner to represent the bulk magnetic properties of a ferromagnetic material is by a plot of magnetic induction B for various field strengths H [48],

$$B = \mu_0(H + M) \ . \tag{1.9}$$

When a ferromagnetic material magnetizes in one direction until the saturation magnetization,then the imposed magnetizing field removed, it will not turn back to zero magnetization. The absence of reversibility of the magnetization curve is the property called hysteresis and it can be related to several factors including the sample shape, surface roughness, microscopic defects and thermal history.The term hysteresis, meaning to slow down ,was introduced by Ewing who was the first who regularly investigate it. Remanence is when the amount of magnetisation field is reduced to zero after magnetizing a magnetic material , the remaining magnetic induction is called the remanent induction B_R and the remaining magnetization is called the remanent magnetization M_R.

$$B_R = \mu_0 M_R \ , \tag{1.10}$$

moreover, it will get back to zero by a field in the opposite direction; the amount of reverse applied magnetic field required to driving to zero the magnetization called coercivity.

The opposite magnetic field is applied until the saturation magnetization, then it is reversed again until saturation at first direction of the applied magnetic field; hence its magnetization will trace out a loop called a hysteresis loop.

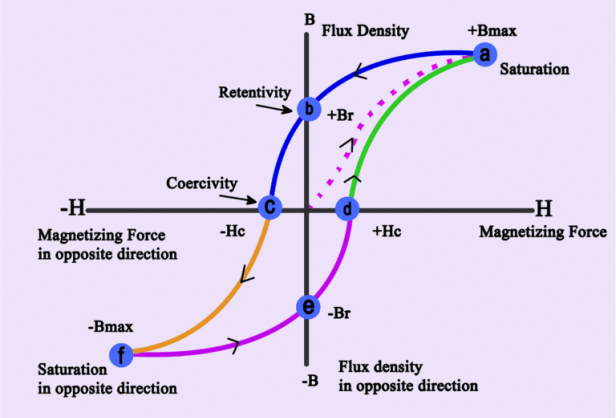


Figure 1.7: Magnetic hysteresis in a ferromagnetic material. Intercepts points H_C and M_R are the coercivity and the remanence respectively

Besides a strong magnetization, the initial magnetization curve,the propriety of ferromagnetic materials for applications is settled principally from characteristics shown by their hysteresis loops (see figure 1.7)[46, 55].

1.5 Magnetic anisotropy

The theory of ferro- and ferromagnetism based on electronic exchange forces. These forces are so strong that these materials are spontaneously magnetized, even in the absence of an applied field. The dependence of magnetic properties on a preferred direction called magnetic anisotropy[55].

Magnetic anisotropic created by the electric field of a solid or crystal, depends on the shape of the magnetic body (to sample or grains shape i.e.; atomic or micro-scale texture), on applied or residual stresses, all of which are characterized by polar vectors[47] .

The main cause that impress the shape of the M, H (or B, H) curve, or the shape of the hysteresis loop ,controls the coercivity and remanence, is magnetic anisotropy.This term simply means that the magnetic properties depend on the direction in which they are measured[56].

Magnetic material said to feature magnetic anisotropy if its internal energy depends on the direction of its spontaneous magnetization regarding the crystallographic axes. Anisotropy is also of considerable practical importance because it is exploited in the design of most magnetic materials of commercial[57].

1.5.1 Magnetocrystalline anisotropy

Magnetocrystalline anisotropy has a key influence on the magnetic properties of most materials, and comes from the electrostatic interaction between the charge distribution of the environment, and the magnetic electron orbital of the atom under investigation.It is an intrinsic property of a ferrimagnet , independent of grain size and shape.In can be most easily seen by measuring magne-

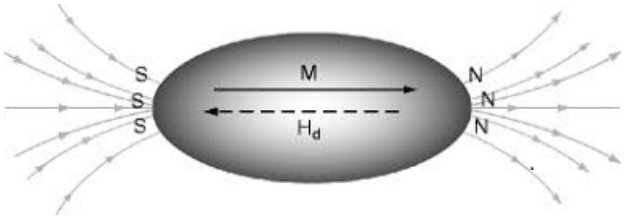


Figure 1.8: Surface magnetic pole and internal demagnetizing field H_d (dashed arrow) for an ellipsoidal grain with uniform axial magnetization M[3].

tization curves along with different crystal directions. Its origin is in the crystal-field interaction and spin-orbit coupling, or else the interatomic dipole-dipole interaction.

The magnetization process is different when the field is applied along with different crystallographic directions, and the anisotropy reflects the crystal symmetry.The phenomenological approach to magneto-crystalline anisotropy consists in considering that energy only depends on the orientation of the magnetic moment (actually the crystalline electric field has an effect also on the modulus of the moment). Depending on the crystallographic orientation of the sample in the magnetic field, the magnetization reaches saturation in different fields. In magnetite, above 130 K [56, 58, 47].

1.5.2 Shape anisotropy

Shape anisotropy mostly occurs in ferromagnetic minerals with high intrinsic susceptibility and low magnetocrystalline anisotropy (e.g., magnetite, maghemite). By analogy with electrostatics, the magnetization M_s creates at the macroscopic scale a field bipolar called the demagnetized field H_d which opposes its orientation (see Fig 1.8). The demagnetizing field (which is the origin of the shape anisotropy) leads to spatial inhomogeneity of the magnetization. Physically, shape anisotropy E_d results from dipole-dipole interactions between the magnetic moments (i.e. non-local energy).whereas magneto-crystalline anisotropy rooted in (local) spin-orbit interaction.

The demagnetized field is zero toward the large dimension and becomes important in direction of a small dimension.The surface magnetic poles generate an internal field whose field lines start on the north magnetic poles on the surface and end on the south poles

This internal field is, therefore, antiparallel to the alignment of the magnetic moments inside the crystal and it is known as the demagnetizing field H_d. Such a demagnetizing field is proportional to the magnetization M of the crystal and is sensitive to its shape:

$$H = -NM \ , \tag{1.11}$$

$$E_d = \frac{-1}{2} N M_s^2 \ , \tag{1.12}$$

where N is a demagnetizing factor that is determined by the shape of each crystal. Shape anisotropy arises from the dependence of the demagnetization factor N on the direction of magnetization regarding the particle shape.

In the nanowires, the shape anisotropy will contribute a term favouring easy axis formation along the wire.the shape anisotropy cannot be an intrinsic property of the material, as it depends on the sample shape[47, 56, 59, 60].

1.6 Spintronic Devices and Magnetoresistance

Spintronics newly emerges in the 1980s concerning spin-dependent electron transport phenomena, based on a combination of three conventional information carriers: an electron charge, an electron spin, and a photon; whereas representing three major fields in information technology (IT); data processing with electron transport, data storage with an assembly of spins and data transfer via optical connections.

Spintronic devices based on the manipulation of spin-polarized electrons offer vast significant advances in device performance in terms of speed, size scaling, and power requirements. The development in this field led to stimulating an increase of the storage capacity besides decreasing the chip area. Noteworthy, Heusler alloys supply a wide range of materials with magnetic properties, many of which are exactly what new data storage technologies require[61, 23].

This mechanism embraces magnetoresistive phenomena such as giant magnetoresistance (GMR) or tunnelling magnetoresistance (TMR). Magnetoresistance is the property of a material to change the value of its electrical resistance when an external magnetic field applies to it. The effect was first discovered by William Thomson (more commonly known as Lord Kelvin) in 1856[62, 63]. whereas, each material system has it MR behaviour and the corresponding ratio, which defined as a percentage of change of MR value regarding the applied magnetic field. Reaching to materials systems with a large MR ratio is the key to develop practical magnetoresistive random-access memory (MRAM),since the large MR effect can improve the memory readout. Because of the higher spin polarization in the half-metallic Heusler compound and alloys, it could replace the existing materials in the applications, including magnetic random access memory (MRAM)[64, 65, 66, 67, 68].

1.6.1 Giant magnetoresistance (GMR)

Thanks to the development of a new growth technique adapted from the semiconductor industry: molecular beam epitaxy (MBE), The growth of such multilayer composed of very thin individual layers to extend the experiments to ternary alloys became possible in the 1980s.In addition, in 1986, Peter Grünberg and co-workers discovered the existence of antiferromagnetic interlayer exchange couplings in multilayer comprising alternating layers of iron and chromium ($Fe/Cr/Fe$)[69, 61].

The electric resistance of a material increases (caused by the Lorentz force) as the applied magnetic field increases, so its affects the motion of conduction electron., i.e., the sign of MR is positive.

The giant magnetoresistance (GMR) effect is the most fundamental phenomenon in spintronics. The origin of the GMR is the dependence of the electrical conduction in ferromagnetic materials on the spin state of the carriers (electrons).

The electric resistance of material changes, once a magnetic field applied to thin films composed of alternating ferromagnetic and nonmagnetic layers. It's called this phenomenon a magnetoresistance (GMR) effect[21].

The slight increase in the spontaneous magnetization leads to the corresponding decrease in electric resistance, and that's because of the appearance of the forced effect under the application of a high magnetic field after saturating the magnetization, which means that the magnetic field works as a tool to switch the relative magnetization of the magnetic layer.

The system would exhibit relatively high resistance when the magnetic moments in neighboring Fe films are antiparallel alignment, with low resistance when they are parallel.The GMR structure has been simplified down to a trilayer comprising ferromagnet (FM)/non-magnet (NM)/FM. Multilayer structures with thin Fe films have a much larger magnetoresistance effect than a single sandwich structure of Fe/Cr/Fe [23].

The GMR was practically used for a read-head of a hard disk drive (HDD) in only 10 years after its discovery. The GMR-based read head had improved the storage density of HDD until GMR was replaced by tunnel magnetoresistance (TMR) later[70, 66, 64, 71].

1.6.2 Tunnel magnetoresistance (TMR)

In 1975, Jullière proposed a simple model to explain the TMR effect in a Magnetic Tunnel Junction (MTJ) , where an ultrathin tunnel barrier is separating two ferromagnetic electrodes. It was the second major discovery in spintronics domain applications of artificial magnetic systems development. The Principle of TMR arises from the spin polarization of conduction electrons at the Fermi surface for ferromagnetic electrodes[21, 66].

A magnetic tunnelling junction (MTJ) comprises a sandwich of two thin ferromagnetic or ferrimagnetic electrodes separated by an ultrathin insulating layer. Whereas, the parameter that measures the transport property of magnetic tunnel junctions with (ferromagnet /insulator /ferromagnet) trilayers is the TMR ratio[61].TMR refers to the change of junction resistance, depending on the magnetic configuration of the electrodes (parallel or antiparallel magnetisation)[72].

With the suppose that the spin-flip scattering is negligible during electron tunnelling, the electrons in an up-spin band move to the other up-spin band whereas the electrons in a down-spin band move to the other down-spin band. The conduction mechanism that lies at the center of TMR structures is dependent on the quantum tunnelling of electrons, which percolate through the non-conductive barrier. Despite the fact that GMR drew research attention towards the domain of spintronics, magnetic tunnel junctions (MTJ) are now found in place of GMR devices within HDD read heads and MRAM applications affording greater magnetoresistance[23, 73, 64, 74].

Chapter 2

Heusler alloy

2.1 Introduction

Heusler compounds reveal different electronic ground states functionalities with important wide-ranging which giving them a significant chance to study and identify their properties in spintronics and exploit them in technology[75, 76].

In 1903, Fritz Heusler made an intriguing discovery of one of the most exciting material classes. He discovered that an alloy, Cu_2MnAl , behaved as a ferromagnet but none of its constituent is a magnetic element. That discovery had grown in the last 100 years, into a family of over 1,000 compounds, synthesized from combinations of over 40 elements and classified under the name Heusler compounds .They are ternary semiconducting or metallic materials with an X_2YZ (also known as full or inverse-Heusler) where X and Y are transition or rare earth elements and Z is the main group element[4, 77].

In the 1980s, electronic and magnetic properties investigation of several Heusler lead to unpredicted results that certain Heusler compounds show metallic as well as insulating properties a feature called half-metallic ferromagnetism ,i.e.the minority band is semiconducting with a gap at the Fermi level EF,while that feature exhibit 100% spin polarization, it made it an ideal candidate for spintronics and magnetoelectronics applications that use the giant and tunnel magnetoresistance effect[4, 76, 78].The half-metallic ferromagnet (HMF) behaves like a metal for one spin direction and like an insulator for the other spin direction.

By counting the number of valence electrons, the properties of many Heusler compounds can be predicted, which provides, the design of semiconductors with tunable band gaps, half-metallic ferromagnet besides other features. Whereas the physical properties and electronic structure of Heusler alloys heavily depend on the structural order degree and distribution of the atoms in the crystal lattice[4, 79, 68, 80].

The Figure 2.1 shows an overview of combinations for the candidate's elements for different types of Heusler alloys.

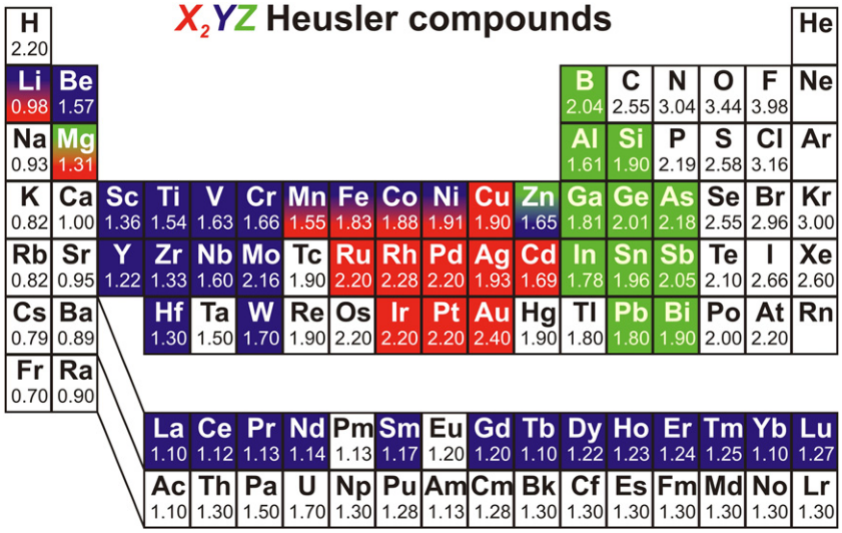
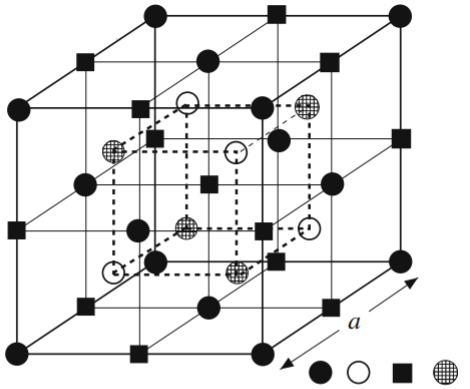


Figure 2.1: Periodic table of the elements. The huge number of Heusler materials can be formed by combination of the different elements according to the color scheme[4]

.



	A	B	C	D
Semi–Heuslers ($C1_b$) : XYZ	X	Y		Z
Full–Heuslers ($L2_1$) : X_2YZ	X	Y	X	Z
Quaternary Heuslers : (XX')YZ	X	Y	X'	Z
Inverse Heuslers (XA) : X_2YZ	X	X	Y	Z

Figure 2.2: Schematic representation of the various structures of the semi- and full-Heusler compounds.[5]

.

2.2 Crystal Structure of Heusler Compounds

The first Heusler alloys studied crystallized in the $L2_1$ structure according to the notation of the Strukturberichte[81] which comprises 4 fcc sub-lattices (see Fig 2.2).

They consider intermetallic compounds with a composition of X_2YZ where X and Y are transitions or rare-earth metals and Z is the main group element. Classical Heusler compounds crystallize with structure type Cu_2MnAl with space group $Fm\bar{3}m$ (No. 225). The X atoms occupy the Wyckoff position 8c (1/4,1/4,1/4), the Y Atoms 4b (1/2,1/2,1/2), and the Z atoms 4a (0,0,0). Instead, it's called a regular Heusler structure.

$C1_b$ structure crystallizes with only 3 sub-latices occupations, under the name of half or semi Heusler (see Fig 2.3).

The quaternary compounds have chemical formula (XX')YZ where X, X', and Y are transition metal atoms.The valence of X' is lower than the valence of X then the valence of the Y element is lower than the valence of both X and X'. The sequence of the atoms along the fcc cube's diagonal is X-Y-X'-Z which is energetically the most stable[82, 76, 4, 5].

For the usual full-Heusler compounds, there are also the so-called inverse Heusler compounds with XA or $X\alpha$ structure, where the series of the atoms is X-X-Y-Z, with the prototype is Hg_2TiCu [83], whereas the atomic number of the X transition-metal atom is smaller than the valence of the Y transition metal and more electropositive than Y [4].

Due to Burch's rule[84], it can be described the observed preferential site occupations. According to this rule, with the X_2YZ structure the X element on the left side in the periodic table, the 8c site in $Fm\bar{3}m$ splits into 4d and 4c in $F\bar{4}3m$. So then, half of the X-type atoms exchange their positions with the Y-type atoms (Li_2AgSb structure type or X-type), $F\bar{4}3m$, no. 216, X on 4d (1/4,1/4,1/4) and 4b (1/2,1/2,1/2), Y on 4c (3/4,3/4,3/4), and Z on 4a (0,0,0)),i.e. X type atoms take the positions 4d and 4c in our case of Mn_2- based Heusler compounds(see Fig 2.4) [12, 4, 5, 7].

2.3 Half-metallic ferromagnet

The primary interest surrounding on magnetic properties in Heusler compounds were the prediction of half metallic ferromagnet (HMF) of the semi Heusler MnNiSb in 1983 by Groot et al.[27, 85], then co_2MnSn by Kubler et al.[86].

The electronic band structure of these materials differs from that of typical metals and semiconductors, It features The minority spin electrons with semiconducting and zero gap behaviour while the majority-spin electrons keep their normal metallic character or spin gapless (see Fig 2.5)[87, 80].

The asymmetric band character reflects the feature that the conduction electrons are (100%) spin polarization at Fermi level. We can define the spin polarization P, that measures the spin

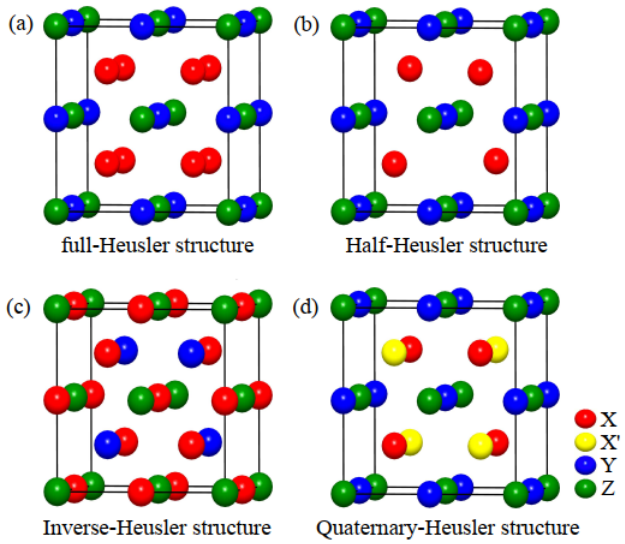


Figure 2.3: Different types of Heusler structures. Full-Heusler (a), Half-Heusler (b),Inverse-Heusler (c), and Quaternary-Heusler structures (d)[6].

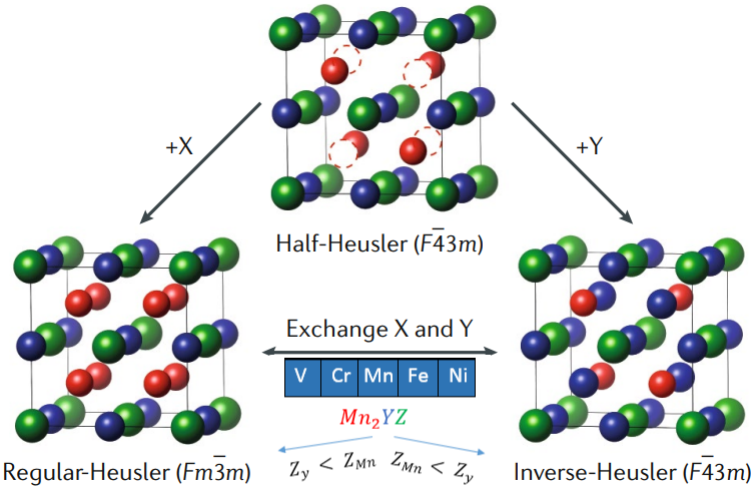


Figure 2.4: Inverse and regular structure for Mn2-based Heusler compounds[6, 7].

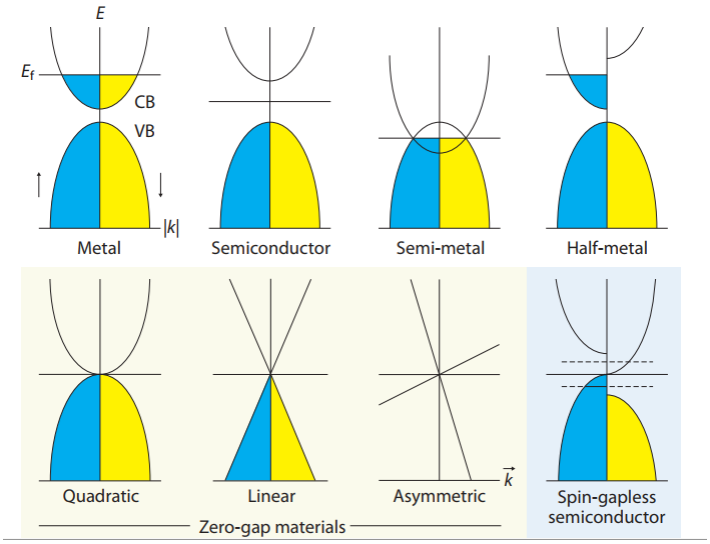


Figure 2.5: The electronic band structures of various classes of materials, metal, semiconductor, half and semi metal[8].

asymmetry[4, 66], by the following expression:

$$P = \frac{\rho\uparrow(E_F) - \rho\downarrow(E_F)}{\rho\uparrow(E_F) + \rho\downarrow(E_F)} \tag{2.1}$$

This exceptional property allow the HMF to be the perfect candidate for spintronic devices such as non volatile magnetic random access memories, magnetic sensors and spin injection device.

Recently, in condensed matter science, Mn-rich Heusler compounds have become the most preferred topic since cubic Mn2-Heusler compounds are half-metallic ferro- or ferrimagnets[5, 88, 82, 68, 27].

2.4 Spin gapless semiconductor

Recently, a new class of materials in the HMF family spin gapless semiconductors (SGS) has emerged. Wang proposed and named the concept of the spin-gapless semiconductor (SGS) in 2008 through the design of its band structure.

Since their theoretical prediction, SGS materials are receiving significant research interest with great expectations in the spintronic devices field. It Supposed as prospective candidates to substitute for diluted magnetic semiconductors (DMS). whereas, it considers as a new class of zero-gap materials that contain fully spin polarized electrons and holes.

SGS materials feature a zero band gap for one spin channel, while a band gap is present for the other channel, as shown in Fig 2.6. Therefore, these materials can serve as a bridge between the HMFs and the semiconductors.

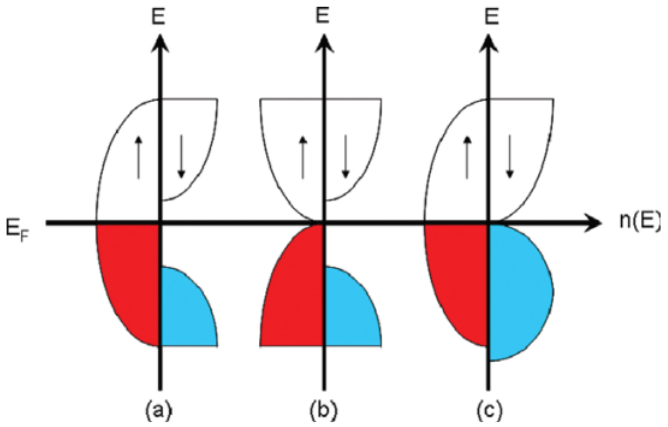


Figure 2.6: The schematic density of states n(E) as a function of energy E is shown for (a) a half-metallic ferromagnet, (b) a spin gapless semiconductor„ and (c) a zero-gap half-metallic ferromagnet. The occupied states are indicated by filled areas. Arrows indicate the majority (↑) and minority (↓) states[9].

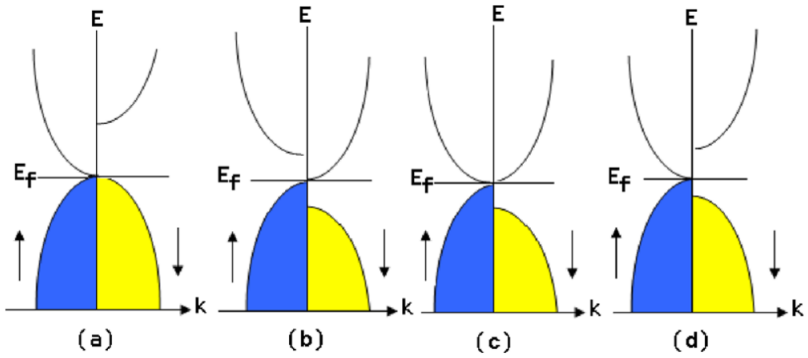


Figure 2.7: Energy band diagrams for spin gapless semiconductors with parabolic dispersion between energy and momentum[8].

Therefore, Wang et al. had proposed four different SGS materials with different configurations of band structures(see Fig 2.7).These are based on gapless semiconductors with parabolic or linear dispersion between energy and momentum(see Fig 2.5). For example, the bottom of the conduction band (C_b) touches the top of the valence band (V_b) at the Fermi level, i.e., the energy gap is zero, and for both electrons and holes are fully spin-polarized case (c) Fig 2.7.

Some of the special properties of SGS are (i) spin-polarized current resulting from electrons as well as spin-polarized holes; (ii) ability to switch between n and p-type spin-polarized carriers by the application of an electric field; and (iii) almost no energy is required to excite electrons from the valence band to the conduction band[89, 90, 91, 92, 93, 94, 8, 95].

Gapless half metallic

Du et al.[9] proposed very recently, a class of materials gapless (also known zero-gap) HM,FM , they theoretically predicted a gapless HM-FM of the inverse Heusler alloy Fe_2CoSi[96]. In gapless HM-FMs, one of the two spin channels is metallic and the other is gapless(see Figure 2.6 (c)). Gapless HM exhibits conducting properties in one of the spin channels(metallic behavior), and almost zero bandgap in the other.

Schematically, when the top of the valence band and bottom of the conduction band touch the Fermi energy for the minority-spin channel but shows a metallic character for the majority spin channel, the resulting band structure is gapless HM.

Mainly, in SGSs and gapless HM-FMs no energy is required to excite electrons from the valence band to the conduction band[97, 96, 98].

2.5 Origin of the Gap

When two atoms approach each other, their electron orbital overlap, which this overlap create a molecular bond between the two atoms with its own molecular orbital shape[99, 100].

The prediction of molecular and electronic properties of a compound requires a vast understanding of the concept of hybridization [101].

The hybridization of atomic orbitals theory is analysed using the principle of superposition by L. Pauling[102].

The study of the origin of the band gap of complete inverse Heusler alloys based on manganese has been introduced according to studies by Skaftouros, et al.[10].

In order to get an idea about the mechanisms concerned, it considers only the d states of double Mn and Fe, which handle the gap at the point Γ, which reflects the structural symmetry in the compound.

The indications e_g, e_u, t_{1u}, and t_{2g} are used as chemical nomenclature that describes the hybrid orbital shape (angular momentum), its coefficients are on the front of the orbitals and give the degeneracy. The characters $d_i = 1, \ldots, 5$ correspond respectively to orbitals d_{xy}, d_{yz}, d_{zx},d_{z^2} and $d_{x^2-y^2}$. The hybridization of Mn(a)-Fe orbitals with the Mn d-orbitals shown in Fig 2.8[103, 26].

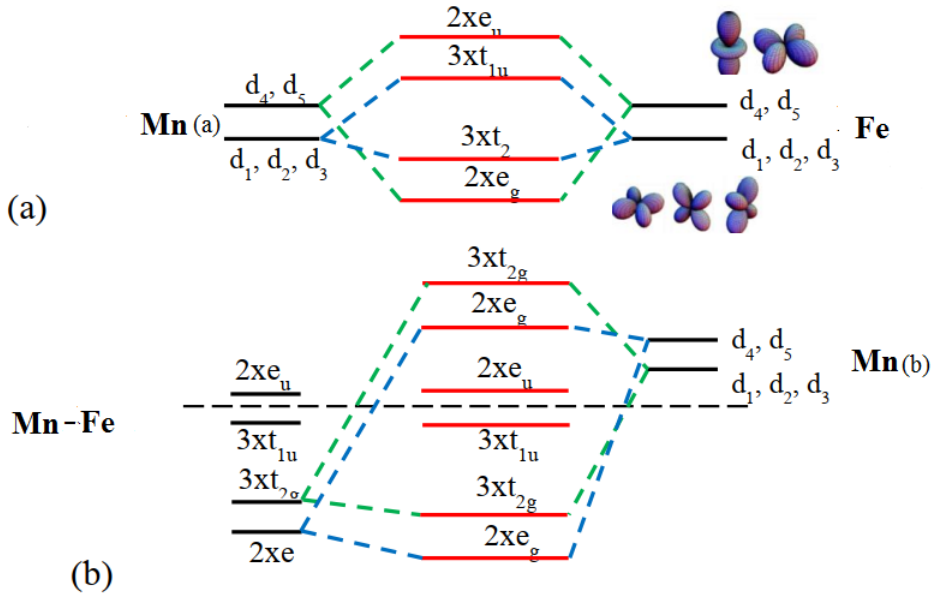


Figure 2.8: Schematic illustration of the origin of the gap in the minority band in inverse-Heusler alloys Mn_2FeSn. The dashed line represents the location of the Fermi level E_F[10, 11].

The 3 d-orbitals of Mn(a) atoms are divided into the twofold degenerate d_{z^2}, $d_{x^2-y^2}$ then threefold degenerate d_{xy}, d_{yz}, d_{zx} states. The e_g orbitals of Mn(a) (t_{2g} orbitals) can only couple with the e_g orbitals (t_{2g} orbitals) of the Fe atom forming new orbitals, hybrid bonding, showed by e_g (or t_{2g}) and the other are anti-bonding orbitals with high energy, indicated by e_u (or t_{1u}).

3d orbits of Mn(a) and Fe hybridized first to create every three states for t_{2g} and t_{1u} ($3 \times t_{2g}$ with $3 \times t_{1u}$) and every two states for e_g and e_u ($2 \times e_g$ with $2 \times e_u$)[104, 105, 106].

The second step of hybridization shows that the $2 \times e_g$ orbital (twofold degenerated) of Mn (a)-Fe hybridizes with the d_4, d_5 orbitals of Mn(b) and forms a bonding orbital (below Fermi level) and another anti-binding (above Fermi level) orbital, both are with $2 \times e_g$ type.

The $3 \times t_{2g}$ orbital (threefold degenerated) of Mn (a)-Fe hybridizes with the d_1, d_2, d_3 orbitals of Mn, three of which are $3 \times t_{2g}$ bonding, settled below the Fermi level and other $3 \times t_{2g}$ anti-bonding above the Fermi level.

The interaction of Mn(a)-Fe with Mn(b) releases five hybridized orbitals ($3 \times t_{1u}$ and $2 \times e_u$) of Mn(a)-Fe. The anti-bonding orbitals $3 \times t_{1u}$ (bottom) and the $2 \times e_u$ (top) are free between the Fermi level. Because Mn (b) atom doesn't have states that represent the same symmetry with the anti-bonding orbitals of Mn(a)-Fe[107].

Then, the e_g and t_{2g} states of the Mn(a)-Fe system are hybridized with Mn(b) 3d states. This hybridization makes XA phase Mn_2FeSn follow the Slater-Pauling's rule: $M_t = Z_t - 24$[10, 106].

As a result, the origin of the energy gap in the minority spin channel dominated by the interaction between the two Mn(a)-Fe atoms and the Mn(b) and Sn atoms. The state of affairs of the five sp bands is much lower than the Fermi level, and these bands have no effect on the gap's

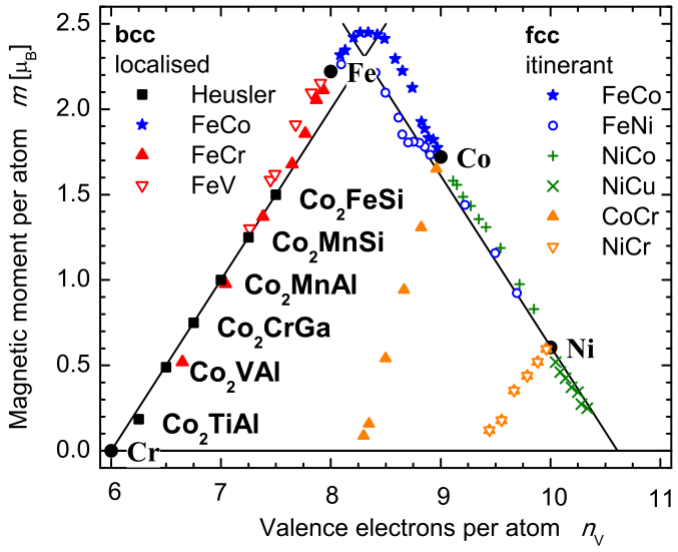


Figure 2.9: The values for 3d transition metals and their alloys are given for comparison[4].

formation. So,the strong hybridization between the d-states of the transition metal atoms is the responsible for the gap[98].

However, the sp orbitals of Sn have affected the positioning of Fermi level, thanks to the participation of its valence electrons in the total valence electrons, which gives it a part in the magnetic properties of the Heusler compound[24, 108, 10].

2.6 The Slater-Pauling rule

Slater[109]and Pauling[110] discovered that the magnetic moment m of the 3d elements and their binary alloys can be estimated based on the average valence electron number (Z_t) per atom[5].

Depending on M (Z_t),using first-principles calculations, the Slater-Pauling rule divided The materials into two areas; The first is the area of low valence electron concentrations ($Z_t \leq 8$) and of localized magnetism, where most bcc structures are found. The second area contains the itinerant magnetism with high valence electron concentrations ($Z_t \geq 8$) where closed packed structures: fcc, hcp are found.whereas, Iron is at the top border between localized magnetism and itinerant magnetism (see Fig 2.9) .

The total number of electrons Z_t is given by the sum of the number of spin-up and spin-down electrons, while the total moment M_t is given by the difference,

$$Z_t = N\uparrow + N\downarrow \tag{2.2}$$

$$M_t = N\uparrow - N\downarrow \tag{2.3}$$

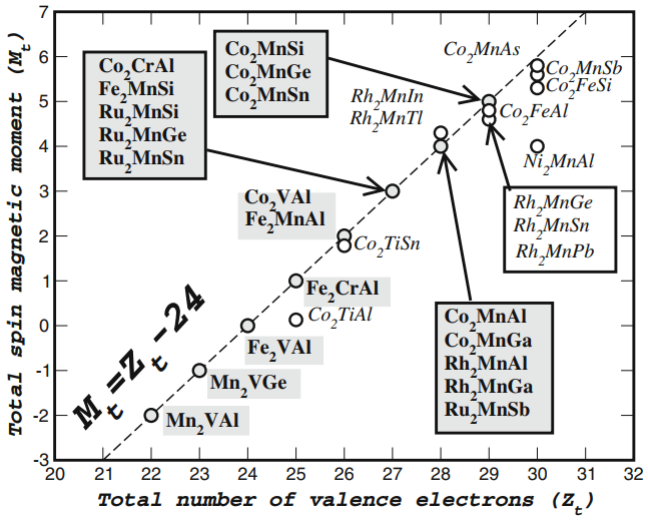


Figure 2.10: Calculated total spin moments for all the studied full Heusler alloys. The dashed line represents the Slater-Pauling behaviour[12].

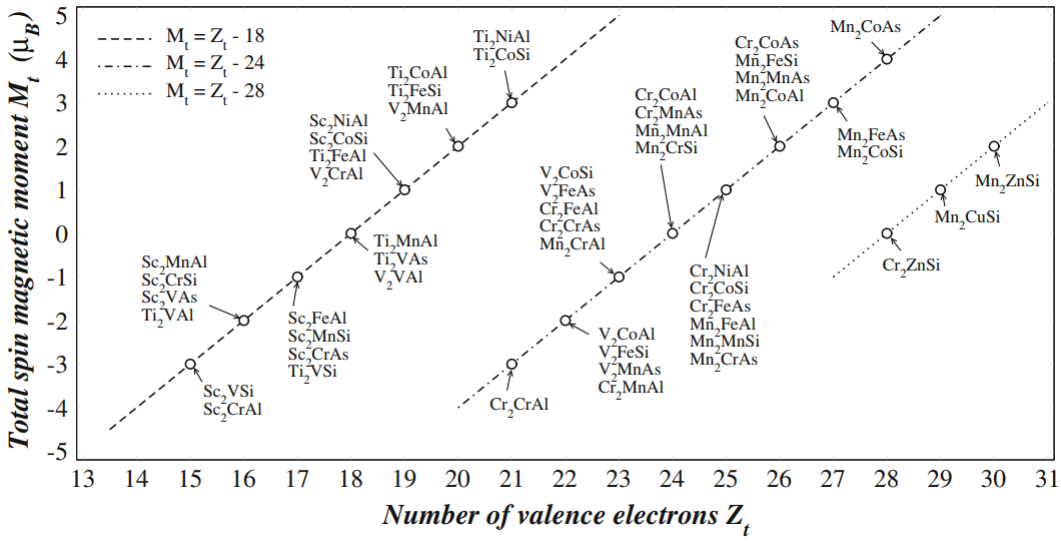


Figure 2.11: Calculated total spin moments for several inverse Heusler compounds studied. The dashed lines represent the three variants of the Slater-Pauling behaviour for these compound[12].

$$M_t = Z_t - 2N\downarrow \tag{2.4}$$

with $N\uparrow$ and $N\downarrow$ are the numbers of electrons in the majority and minority states, respectively.

The figure 2.9 shows the Slater-Pauling curve for transition metals. The local part of this curve carries Heusler compounds. Thus, The magnetic moment in multiples of Bohr magneton μ_B is given by:

$$M_t = Z_t - 2N\downarrow \tag{2.5}$$

Where $2n\downarrow$ signifies the number of electrons in minority states. In the $d\downarrow$ minority band, the minimum number of electrons is about three. Ignoring the contributions of s and p electrons, the magnetic moment in the localized area of the Slater-Pauling curve , the equation becomes:

$$M_t = Z_t - 6 \tag{2.6}$$

where Z_t is the total number of valence electrons in the unit cell.

For semi-Heusler XYZ compounds, which comprise three atoms per primitive cell (formula unit) , the Slater-Pauling rule is given by :

$$M_t = Z_t - 18 \tag{2.7}$$

The figure 2.10 represent the total spin magnetic moments for all the compounds under study as a function of the total number of valence electrons with a dashed line which describe the half metallicity rule:

$$M_t = Z_t - 24 \tag{2.8}$$

for the full Heusler alloys.

The concept of that rule is that the minority band contains 12 electrons per unit cell: 4 are occupying the low-lying S and P bands of the sp element and 8 for the Mn minority d bands , as explained above (see Fig 2.8).

Thence, for several of inverse Heusler compound ,that shown in figure 2.11 ,when X is Sc or Ti the total spin magnetic moment per formula unit (or unit cell) in μ_B follows the rule $M_t = Z_t - 18$

When X = Cr, Mn or V , the variant followed by M_t like the full Heusler compounds equation 2.8 that argued above. The explication of the appearance of these rules depends on simple hybridization arguments of the transition metal d-orbitals.

At last, it has concentrated on the compounds that the X is Cr or Mn and Y is Cu or Zn, that half-metallic compound follows the rule[4, 111, 10, 112, 113, 90, 95, 24].

$$M_t = Z_t - 28. \tag{2.9}$$

Chapter 3

Foundations of the density functional theory

3.1 Introduction

Understanding and controlling the properties of matter at individual levels of atoms molecules; is the key to scientific and technological progress in physical-chemical sciences.

Modern methods of calculating solid-state properties are based on quantum theory, where the computations are by many-body interactions among electrons and nuclei.

solid-state physicists carried out the calculation of the electronic structure which consider as the first effective tool for understanding the relationships between crystallographic structures and Physics-chemical properties.

The ab initio methods have been developed to become today an essential tool in the structural, electronic, elastic properties and optical systems of the most complex systems and their physical properties. They are considered as a tool to predict a new material and sometimes could replace very expensive or even impractical experiments in the laboratory.

In the last two decades, density functional theory (DFT) calculations are quickly becoming a "standard tool" for various materials modelling problems in physics, chemistry, materials science, and multiple branches of engineering.

Density functional theory is a successful approach thanks to its great accuracy and lower computational costs, it found solutions to the fundamental equation that describes the quantum behaviour of atoms and molecules, the Schrödinger equation.

Ab initio calculations are performed using the pseudo-potential approximation and plane wave method (PP-PW) in the framework of density functional theory (DFT).

There are a large number of calculation codes based on this method, one cites as example WIEN2K, Dmol3 (Delley, 1990), VASP (Kresse and Furthmüller, 1996), GAUSSIAN (Gaussian 03), ABINIT (Gonze et al. 2002), CRYSTAL (Dovesi et al. 2010), Big DFT (GENOVESE et al. 2009)[114, 115, 116, 117, 118, 119, 120].

3.2 Schrödinger equation

In 1925, the Austrian physicist Erwin Schrödinger created an equation bearing his name, which today is one of the pillars of quantum mechanics. It describes the evolution of a non-relativistic particle over a period of time. Thus it plays the same role as the fundamental relationship of dynamics in classical mechanics[121, 122, 120].

The theoretical study of the physical properties of materials requires the solution of the equation of Schrödinger independent of time, given by the following relation :

$$\hat{H}\Psi_i(\vec{r_i},\vec{R_i}) = E\Psi_i(\vec{r_i},\vec{R_i}) \tag{3.1}$$

where;
$\hat{H}$: is the Hamiltonian of the system.
Ψ_i : the wave function of the system.
$\vec{r_i}$: The variables describing electron positions i.
$\vec{R_i}$:The variables describing nuclei positions (Cartesian coordinates).
E : is the energy eigenvalue for the stationary state described by ψ the wave function[118].
Usually, the Hamiltonian operator is written as :

$$\hat{H} = \hat{T}_e(r) + \hat{T}_n(R) + \hat{V}_{e-e}(r) + \hat{V}_{n-n}(R) + \hat{V}_{n-e}(R,r) \tag{3.2}$$

$\hat{T}_e$ and $\hat{T}_n$; electrons and nuclei kinetic energy operators ,

$$\hat{T}_e = \frac{-\hbar^2}{2m}\sum_{i=1}^{N}\nabla_i^2 \tag{3.3}$$

$$\hat{T}_n = \frac{-\hbar^2}{2M}\sum_{\alpha=1}^{K}\nabla_\alpha^2 \tag{3.4}$$

the potential operator $\hat{V}_{n-n}$ represents the repulsion among the nuclei,

$$\hat{V}_{n-n} = \frac{ke^2}{2}\sum_{\alpha,\beta=1,\alpha<\beta}^{K}\frac{Z\alpha Z\beta}{|R_\alpha - R_\beta|} \tag{3.5}$$

$\hat{V}_{e-e}$; the operator of energy interaction among the electrons,

$$\hat{V}_{e-e} = \frac{ke^2}{2}\sum_{i,j=1,i<j}^{N}\frac{1}{|r_i - r_j|} \tag{3.6}$$

$\hat{V}_{n-e}$; the operator of interaction between electrons and nuclei.

$$\hat{V}_{n-e} = -\frac{ke^2}{2}\sum_{\alpha=1}^{K}\sum_{i=1}^{N}\frac{Z\alpha}{|R_\alpha - r_i|} \tag{3.7}$$

m: the mass of the electron. M: the mass of the nucleus. The labels i, j, α and β denotes the particles coordinates . The wave function ψ of N electrons depends on 3N spatial coordinates besides N spins coordinates, which makes it impossible to solve the equation 3.1. So this surely guides us to use some approximations.

3.2.1 Born Oppenheimer approximation

The Born-Oppenheimer approximation[123], proposed in 1926, is considered the most important in quantum chemistry, as it is theorized the first constant approximation aimed at simplifying the Schrödinger equation.

It allows us to manipulate the electronic structure of molecules very precisely without worrying that the nuclei. It is based on the separation of the movement of electrons from the movement of atomic nuclei based on the huge difference between the masses of the nucleus and the electron, which is a doubled coefficient of about 1836.

So that the nuclei have a movement much slower than the movement of electrons. To reach the approximation, it was taken into account that the electrons of the molecule move in a fixed nucleus field, meaning that the kinetic energy of the nucleus is neglected $\hat{T}_n$ =0.

then we can write the wave function of the system in the form of the product of two distinct wave functions, one for the nucleus (the nuclear term $\Psi_n(\vec{R})$) and the other for electrons (the electronic term $\Psi_e(\vec{r})$).

$$\Psi(\vec{R},\vec{r}) = \Psi_n(\vec{R})\Psi_e(\vec{r}) \tag{3.8}$$

The potential energy V_{n_n} is considered constant. We, therefore, consider that the electrons move in a field created by fixed atoms. Thus, the electronic and nuclear Hamiltonians are written as;

$$\hat{H}_e = \hat{T}_e(r) + \hat{T}_{e_e}(r) + \hat{T}_{n-e}(R,r) \tag{3.9}$$

$$\hat{H}_n = \hat{V}_{n-n} = constant \tag{3.10}$$

Although it is impossible to dispense with this approximation in the calculations of the molecular wave functions, it is severe to solve the equation due to the difficulties of the electronic motions and the interactions that control it. To overcome this difficulty, a series of approximations must be made[124, 125, 33, 126].

3.3 Density functional theory

At the end of the 1920s, both Llewellyn Thomas[127] and Enrico Fermi[128] developed the density functional theory, which is today one of the most widely used methods for quantum computations of the electronic structure of matter, which states that the electronic properties of a system can

be calculated through its density electronic, Under the assumption that the electron density is homogeneous, they are the first who deal with electronic interactions and kinetic energy.

However, it did not take into account all the efforts presented until the mid-sixties, due to the contributions of Hohenberg and Kohn, then Kohn and Sham[129], that model has been developed which establish the theory in force today.The main purpose of DFT is to replace the function of the multi-electronic waves with electron density. As known that the electron density in an electronic system is the number of electrons per unit volume in a given state (or the probability of finding an electron in a unit volume), defined by:

$$\rho(\vec{r}) = N \int ... \int |\Psi(\vec{x}_1,\vec{x}_2,....\vec{x}_N)|^2 d\sigma_1 d\sigma_2 ... d\sigma_N \tag{3.11}$$

This density is equal to zero when r tends to infinity and is equal to the total number of electrons N when integrated throughout space[130, 120, 131, 132].

$$\rho(\vec{r} \to \infty) = 0 \tag{3.12}$$

$$\int \rho(\vec{r}) d\vec{r} = N \tag{3.13}$$

3.4 Hohenberg and Kohn's theorem

In 1964 by Hohenberg-Kohn[133] a DFT suitable for manipulating interacting electron systems was developed on the basis of a study that showed a bijection match between the external potential V_{ext} and the electronic density $\rho_0(\vec{r})$.

Through that density, All properties of a system in its fundamental state could be determined, which is obtained by the covariance principle applied to the functional energy of the system[132, 134, 120].

3.4.1 First Hohenberg-Kohn Theorem

Hohenberg and Kohn showed that for a particles system interacting with an external potential V_{ext} , it consider as a function of electron density.

The arrows indicate the relation obtained in the case of the traditional solution of the Schrödinger equation where the knowledge of the external potential $V_{ext}(\vec{r})$ will make it possible to determine the different electronic states (i.e. the wave functions ψ_i) but also the essential state and the electron density associated with it.

In the ground state the electron density $\rho_0(\vec{r})$ determines the external potential $V_{ext}(\vec{r})$ of the nuclei,which determines the Hamiltonian H then the wave function $\Psi_0(r)$, knowing that the electron density in the ground state is sufficient to obtain all the properties of the device . The first HK theorem, shown, serves to complete this cycle.

$$\rho_0(\vec{r}) \to V_{ext} \to \Psi_0(r) \to \rho_0(\vec{r}) \tag{3.14}$$

3.4.2 Second Hohenberg-Kohn Theorem

This theorem shows that the energy functional $E[\rho(\vec{r})]$ is minimum when any electronic density $\rho(\vec{r})$ corresponds to the electronic density of the ground state $\rho_0(\vec{r})$.

$$E[\rho_0(\vec{r})] = E[\rho(\vec{r})] \tag{3.15}$$

The physical (or « real ») electron density of a system is the one minimising the total energy functional of the system (variational principle), whereas it is possible to write the energy of the system as a function of the electronic density.

$$E[\rho(\vec{r})] = F_{HK}[\rho(\vec{r})] + \int V_{ext}(\vec{r})\rho(\vec{r})d\vec{r} \tag{3.16}$$

with F_{HK} is the universal functional which is valid for any system of electrons:

$$F_{HK}[\rho(\vec{r})] =< \Psi|T_e + V_{e-e}|\Psi > \tag{3.17}$$

For each specific $V_{ext}(\vec{r})$, the energy of the ground of the device is the value which minimizes this functional, the density $\rho(\vec{r})$ associated with it corresponds to the exact density $\rho_0(\vec{r})$ of the ground state.

In end, the two proposed theorems by Hohenberg and Kohn allow to remove the posed problem by the solution of a multi-electronic Schrödinger equation. Indeed, the DFT method informs us that if the shape of the functional is known, it is easy, for a given external potential, to determine the energy of the ground state. in the other side the term $F_{HK}[\rho(\vec{r})]$ has no indication that's why we need other approximations to solve the problem[118, 120, 135, 136].

3.5 Kohn and Sham theorem

In 1964, Walter Kohn and Lou Joe Sham[129] proposed a solution to the problem left by Hohenberg and Kohn's theory by replacing the real system of interacting electrons by a non-interactive imaginary system. It consists of n independent electrons interacting with the external potential. In order to reach the total energy of the electronic system and the density of the ground state charge (see Fig 3.1), from which all other physical properties can be extracted[13, 118].

According to the first theorem of Hohenberg and Kohn[133], the functional $E[\rho(\vec{r})]$ can be written according to the expression:

$$E[\rho(\vec{r})] = T[\rho(\vec{r})] + V_{e-e}[\rho(\vec{r})] + \int V_{ext}(\vec{r})\rho(\vec{r})d\vec{r} \tag{3.18}$$

The Kohn and Sham theorem is consists with rewriting the Hamiltonian of the system with the interacting particles and non-interacting particles,means that the idea was to split these implicit

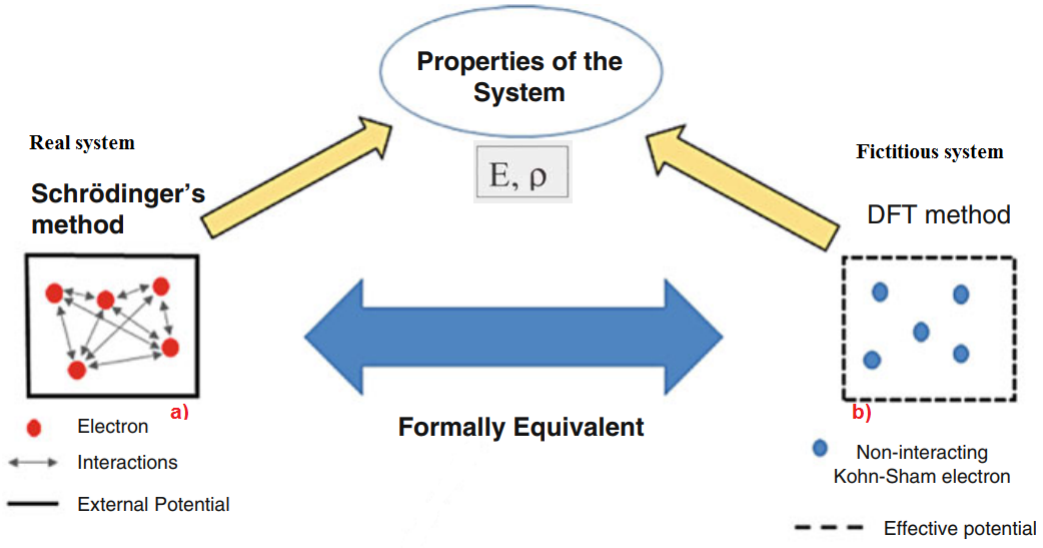


Figure 3.1: Diagram illustrating the concept of interactive real system and the non-interactive fictitious system ; (a): Real system made up of several electrons in mutual interaction; (b): fictitious system of independent fermions with the same energy and the same electron density as the real system[13, 14].

.

terms into the kinetic and Coulomb energy of independent electrons plus an extra term which accounts for the difference:

$$E[\rho(\vec{r})] = \underbrace{T_s[\rho(\vec{r})] + E_{Hartree}[\rho(\vec{r})] + \int V_{ext}(\vec{r})\rho(\vec{r})d\vec{r}}_{\text{Total energy in the independent electrons approximation}} + \overbrace{\underbrace{[T[\rho(\vec{r})] - T_s[\rho(\vec{r})]] + [E_{e-e}[\rho(\vec{r})] - E_{Hartree}[\rho(\vec{r})]]}_{\text{Total energy in the Interacted electrons approximation}}}^{E_{xc}[\rho(\vec{r})]} \tag{3.19}$$

The extra term, $E_{xc}[\rho(\vec{r})]$, contains everything that is left out and is called the exchange and correlation energy (i,e.This term contains all the differences between the non-interactive fictitious system and the real interactive system) including corrections for both the Coulomb interaction and the kinetic energy.

$$E[\rho(\vec{r}) = T_s[\rho(\vec{r})] + E_{Hartree}[\rho(\vec{r})] + \int V_{ext}(\vec{r})\rho(\vec{r})d\vec{r} + E_{xc}[\rho(\vec{r})] \tag{3.20}$$

With : $T_s[\rho(\vec{r})]$: is the kinetic energy of the gas of non-interacting electrons or the energy of non-interactive Kohn-Sham fermions,

$$\rho(\vec{r}) = \sum_{i=1}^{N} |\Psi_i(\vec{r})|^2 \tag{3.21}$$

$$T_s[\rho(\vec{r})] = \frac{\hbar^2}{2m} \sum_{i=1}^{N} |\Delta\Psi_i(\vec{r})|^2 \tag{3.22}$$

$E_{Hartree}[\rho(\vec{r})]$: is the classical Coulomb interaction energy between electrons (electrons repulsion energy) written in terms of their charge density[120, 118, 132, 117].

$$E_{Hartree}[\rho(\vec{r})] = \frac{1}{2}\int\int \frac{\rho(\vec{r})\rho(\vec{r'})}{|\vec{r}-\vec{r'}|}d\vec{r}d\vec{r'} \tag{3.23}$$

Where H_{KS} is the Kohn-Sham Hamiltonian defined by:

$$H_{KS} = \frac{-\hbar^2}{2m_e}\vec{\nabla}_i + V_{eff}(\vec{r}) \tag{3.24}$$

$$H_{KS} = T_e + V_{eff}(\vec{r}) \tag{3.25}$$

With the effective potential:

$$V_{eff}(\vec{r}) = V_{e-e}[\rho(\vec{r})] + V_{ext}[\rho(\vec{r})] + E_{xc}[\rho(\vec{r})] \tag{3.26}$$

The Kohn - Sham mono-electronic equations will be of the form:

$$[H_{KS}(\vec{r}) - \epsilon_i]\psi(\vec{r}) = 0 \tag{3.27}$$

3.6 Exchange-correlation approximations

The benefit of the Kohn-Sham equation is that it contains wave functions of non-interacting particles, and terms that can be determined explicitly (kinetic energy and classical Coulomb potential) have been separated from the unknown exchange and correlation energy.

Non-classical many-body effects are gathered together in the correlation and exchange functional. This makes the problem tractable.

Since $V_{xc}[\rho(\vec{r})]$ is the only unknown term, approximations of it can be made to a reasonable degree of accuracy. Correlation and exchange are so important, Without it, the calculated values of cohesion would be much lower than in reality[137, 138].

The potential for exchange and correlation given by the derivative of the functional:

$$V_{xc}[\rho(\vec{r})] = \frac{\partial E_{xc}[\rho(\vec{r})]}{\partial[\rho(\vec{r})]} \tag{3.28}$$

The most widely used approximations are the local density approximation (LDA), the local spin density approximation (LSDA) and the generalized gradient approximation (GGA).Among the main approximations, we can cite;

3.6.1 The Local density approximation (LDA)

In the Local Density Approximation[139], it is assumed that the electron density can be processed locally as a gas uniform electrons. In other words, this approach consists of making the following two assumptions:

1- the exchange-correlation effects are dominated by the density located at the point $\vec{r}$;

2- the density $\rho(\vec{r})$ is a slowly varying function with respect to $\vec{r}$.

Thus, the fundamental assumption contained in the formalism of the LDA consists in considering that the contribution of $E_{xc}[\rho(\vec{r})]$ to the total energy of the system can be added cumulatively from each portion of the non-uniform gas as whether it was locally uniform[140, 138].

The LDA exchange-correlation functional assumes that the correlation exchange part of the total energy of the ground state of the electronic system can be written according to the expression:

$$E_{xc}^{LDA}[\rho(\vec{r})] = \int \rho(\vec{r})\varepsilon_{xc}[\rho(\vec{r})]d\vec{r} \tag{3.29}$$

In which $\varepsilon_{xc}^{LDA}[\rho(\vec{r})]$ represents the exchange-correlation energy per electron in a system of mutually interacting electrons of uniform density $\rho(\vec{r})$;

$$\varepsilon_{xc}^{LDA}[\rho(\vec{r})] = \varepsilon_{x}^{LDA}[\rho(\vec{r})] + \varepsilon_{c}^{LDA}[\rho(\vec{r})] \tag{3.30}$$

From $\varepsilon_{xc}^{LDA}[\rho(\vec{r})]$, the exchange-correlation potential) $V_{xc}^{LDA}(\vec{r})$ can be obtained in a variational way according to the equation :

$$V_{xc}^{LDA}(\vec{r}) = \frac{\delta(\rho(\vec{r})\varepsilon_{xc}^{LDA}[\rho(\vec{r})])}{\delta\rho(\vec{r})} \tag{3.31}$$

The exchange energy for a uniform electron gas is given by Dirac's formula[141] with the following equation;

$$\varepsilon_{x}^{LDA}[\rho(\vec{r})] = -C_x\rho^{1/3}(\vec{r}) \tag{3.32}$$

3.6.2 Generalized gradient approximation (GGA)

A first step carried out with the objective of improving the processing of exchange-correlation energy consists in making the functional $E_{xc}[\rho(\vec{r})]$ dependent not only on the electron density but also on its gradient $|\nabla\rho(\vec{r})|$.

Thanks to this modification[142], the functional $E_{xc}[\rho(\vec{r})]$ accounts for the non-uniform character of the electron gas. In contrast, GGA functionals cannot be considered as non-local methods given that they depend only on the density (and its first derivatives) at a given point.

In the GGA formalism, the contribution of $E_{xc}[\rho(\vec{r})]$ to the total energy of the system can be added cumulatively from each portion of the non-uniform gas as if it were locally non-uniform[138, 118]. This definition of the GGA functional implies that it is of the form:

$$E_{xc}^{GGA}[\rho(\vec{r})] = \int \varepsilon_{xc}[\rho(\vec{r}),|\nabla\rho(\vec{r})|]\rho(\vec{r})d\vec{r} \tag{3.33}$$

In which $\varepsilon_{xc}[\rho(\vec{r}),|\nabla\rho(\vec{r})|]$ represents the exchange-correlation energy per electron in a system of interacting electrons of non-uniform density.

3.6.3 PBEsol exchange-correlation functional from Perdew–Burke– Ernzerhof approximation (GGA)

Popular GGAs represent a good balance between computational efficiency, numerical accuracy, and reliability, whereas PBE also juggles the demands of quantum chemistry and solid-state physics.

One of the most popular GGA XC functionals is the PBEsol[143] functional approximation, which is used in many electronic-structure calculations in condensed-matter physics and materials science. This approximated functional describes well the short-range correlation, showing important binding in layered materials.

Other equilibrium properties, such as bulk modulus, phonon frequencies, magnetism, and ferroelectricity, are sensitive to the lattice constant, and so are also overcorrected by PBE.

PBEsol is exact for the uniform gas, and highly accurate for large jellium clusters, both of moderate and high density. in addition, PBEsol also becomes exact for solids under intense compression, where real solids and their surfaces become truly slowly varying, and exchange dominates over correlation[144, 145].

3.7 Solving the Kohn-Sham equations

The KS equations are restated here as;

$$(-\frac{1}{2}\nabla^2 + v_{ext}(r) + v_H[\rho^{in}(r)](r) + v_{xc}[\rho^{in}(r)](r))\phi_i(r) = \varepsilon_i\phi_i(r), \tag{3.34}$$

$$\rho^{in}(r) = \sum_{i\in occupied} |\phi_i(r)|^2, \tag{3.35}$$

considering a local exchange-correlation potential.

Therefore, in order to even begin solving the above system of equations, one must estimate an initial electron density to use as input,ρ^{in}.

Once an initial input density has been specified, the (linear) KS equations can be solved Eq 3.34. The output electron density found,from these single particle orbitals, ρ^{out} , is constructed using Eq 3.35. In general, the input and output densities are equal if it has found the ground-state electron density that solves the KS system.

The computational of iterative method (self-consistent field method) start from an initial guess electron density, to get the electron density that solves the KS system.This process is summarised in Fig 3.2.

Solving this system amounts to finding a fixed point of the non-linear KS diagram, $\rho^* = \rho^{in} = \rho^{out}$, which based on utilizing the iterative procedure that acts to define a sequence, $\rho_1^{in},...,\rho_n^{in}$, such that $\rho^* = \rho_n^{in}$ within some defined tolerance.

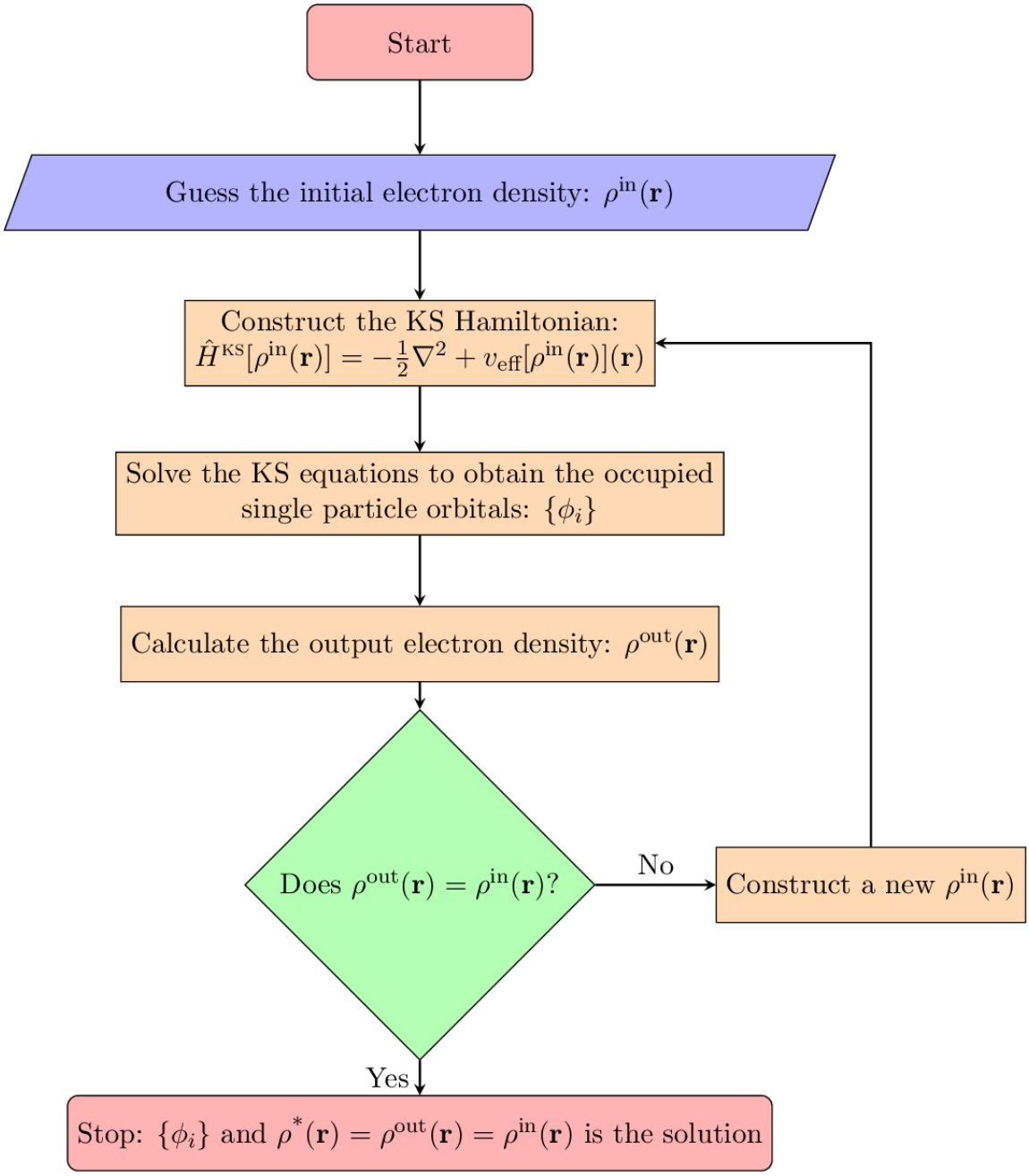


Figure 3.2: Schematic representation of the self-coherent cycle within the framework of the Functional Theory of Density. The electron density constitutes the fundamental quantity which governs the iterative procedure by defining both the starting point and the end point of the self-coherent cycle[15].

.

This sequence is generated as strongly and efficiently as possible, which is to say, the sequence will eventually converge, and it does so much that n is minimised.

3.8 Bloch's theorem and plane wave basis set

To calculate the total energy of solids, the plane wave expansion of the Kohn Sham wave functions is very useful because it takes advantage of crystal lattices repeating periodically in all three directions of space and in an infinite manner.

Due to the orthogonalization to the inner electronic wave functions, The valence wave functions of the large Z atoms oscillate strongly in the vicinity of the atomic core.

There is a difficulty in calculating the total energy because of the perturbations and oscillations that require a large number of plane waves.

Many disturbances are caused by the inner electrons, which are considered inert and have little effect on bonding. Therefore, an atom is described based on its valence electrons only through the so-called pseudo-potential approximation[146, 147].

In bulk crystalline systems, the periodicity of the effective potential is straightforward and can be expressed as the condition[136]:

$$u_i(\vec{r} + \vec{R}) = u_i(\vec{r}) \tag{3.36}$$

where R is a translation vector of the crystal lattice (Bravais lattice).

In 1929. Bloch[148] presented a theory expressing the single-electron wave function ψ_i in a crystal, where the potential is periodic u(r), in the form of the product of plane waves by a function $u_i(\vec{r})$, if r has a periodicity in the crystal lattice of the solid system:

$$\psi_i(\vec{r}) = u_i(\vec{r}) e^{i\vec{k}\vec{r}} \tag{3.37}$$

With k is any allowed wave vector for the electron of the first *Brillouin* zone (BZ).

The function $u_i(\vec{r})$ can be developed on a discrete basis of plane waves whose wave vectors are $\vec{G}$ vectors of the reciprocal lattice of the crystal structure :

$$u_i(\vec{r}) = \sum_G C_{i,G}\, e^{i\vec{G}\vec{r}} \tag{3.38}$$

So, the general expression of the wave function ψ_i can be written in the following form [149];

$$\psi_i(\vec{r}) = \sum_{G=0}^{\infty} C_{i,k+G}\, e^{i(\vec{G}+\vec{k})\vec{r}} \tag{3.39}$$

Bloch's theorem allows us to take an infinite system but only to calculate a finite number of electronic wave functions. However, this leaves an infinite number of k points so that each electron occupies a specific k. whereas the electron wavefunctions at these near k points are nearly identical. So the k-space region is represented by the wave function at a single k point.

In order to achieve this effective k point sampling (geometric optimization), methods for performing discrete sampling of the space of points k have been developed (e.g. Monkhorst and pack[150], Chadi and Cohen[151], Joannopoulos and Cohen[152], Evarestov and Smirnov[153]). The first method is the one that is used in our calculations in *Castep* code.

The Network symmetry has been used to reduce the number of k points required. Further, the Brillouin zone can be made irreducible by applying the point set symmetries of the network, without leaving k points associated with the symmetry.

A cutoff energy value, E_{cut}, determines the number of PWs (N_{pw}) in the expansion, satisfying,

$$\frac{\hbar^2}{2m}|k+G|^2 \leq E_{cuttof} \tag{3.40}$$

N_{PW} is a discontinuous function of the PW kinetic energy cutoff, while depends only on the computational cell size and the cutoff energy value.

i.e.it takes into account all plane waves whose kinetic energy is greater than or equal to the highest kinetic energy of the plane waves used. This corresponds to a sphere in reciprocal space within which all the users $|k+G|^2 \leq E_{cuttof}$ vectors lie[154].

For each of the k vectors, the use of plane waves in the Cohen and Sham equations provides a solution of a system of equations of the following form:

$$\sum_{\vec{G'}}[\frac{\hbar^2}{2m}|\vec{k}+\vec{G}|\delta_{GG'}+V_{ext}(\vec{G}+\vec{G'})+V_H(\vec{G}+\vec{G'})+V_{xc}(\vec{G}+\vec{G'})]C_{i,\vec{k}+\vec{G'}}=\epsilon_{i,k}C_{i,\vec{k}+\vec{G'}} \tag{3.41}$$

The number of allowed wave vectors in a primitive cell of the reciprocal lattice is equal to the total number of lattice sites in the crystal.

Bloch's theorem thus makes it possible to transform the problem consisting in solving an infinite number of mono-electronic equations into that of solving a finite number of mono-electronic equations for an infinite number of points k in a finite volume (Brillouin zone)[155, 156, 147, 157, 158].

3.9 pseudos-potentials Method

Sommerfeld's free-electron model[159] gave a reasonable picture of some chemical properties , by Taking into account the valence electrons and completely disregarding both the core electrons and the nuclei, which was the starting point for introducing the concept of pseudopotential.

The basic idea of the pseudopotential method goes back to Fermi[160] In 1934, which proposed a method to describe the study of observed atomic levels by replacing the complex effects of the core electrons with an effective potential described by the pseudo-wavefunctions of the valence electrons.

In the same year, soon after, this pseudopotential, was achieved by Hellmann[161] who implemented it to describe the energy levels of alkali atoms[162, 163].

In 1959, Phillips Kleinman and Antoncik[164, 165] developed the pseudopotential method that is widely used to calculate the band structure of solids.

Phillips-Kleinman cancellation theorem has shown that valence electrons experimentally exhibit a repulsive potential when they are outside the core; means that their wave functions are forced to be orthogonalized to the states of the heart.

In a solid system, the ability to affect the valence electron is very attractive inside the core. In this area, the wave function oscillates so rapidly due to the electrons of the core that it is difficult to represent it on a plane wave basis (see Fig 3.3).

As known most physical properties of solids are dependent on the valence electrons to a much greater extent than on the core electrons.

The basic concept of pseudopotential (PP) was based on replacing the Coulomb strong potential of the nucleus and its core electrons with an effective ionic potential acting on the valence electrons which is described by pseudo-wavefunctions, rather than the true valence wave functions.

In the sense of collecting the core electron 'frozen' with the nuclei together and consider them as rigid non-polarizable ion cores under the term $(frozen - core - approximation)$.

The pseudo-potential approximation allows the electronic wave functions to be expanded using a much smaller number of plane-wave basis states and diminishing the time calculation.

The main idea of this approximation is to represent the atom as a sphere with a cut-off radius for each pseudo orbital (r_c), whereas the constructed pseudo-potential and the pseudo wave functions match with the real potential and to the real wave functions. Due to this approximation, the potential and wave functions softened in order to remove the perturbation and oscillations. There are several types of pseudo-potentials and the one used in our calculations is The ultra-soft pseudo-potentials introduced by Vanderbilt[166] and presented in CASTEP code[167, 168, 155, 33].

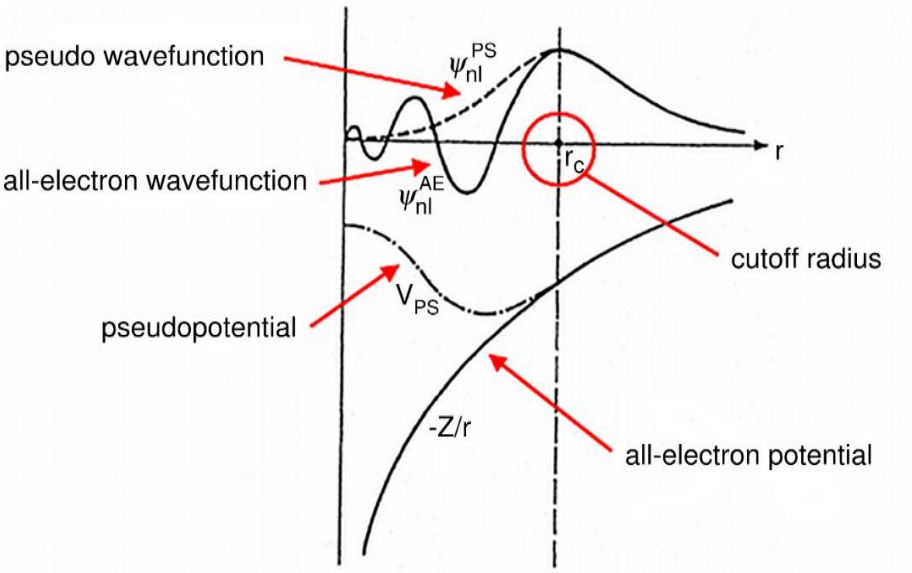


Figure 3.3: Schematic illustration of all-electron (solid lines) and pseudo electron (dashed lines) potentials and their corresponding wave functions[16]. The radius at which all-electron and pseudo electron values match is designated r_c.

Chapter 4

Results and discussions

Introduction

Heusler alloys are interesting as they can support, spin polarization which is highly desired to improve the performance of spintronics devices that is indispensable for the advance of modern technology[169].

In this chapter, as a first step is to determining the structure corresponding to the most stable phase for the inverse Heusler Mn_2FeSn, followed by a study of structural, electronic and magnetic properties of this optimized phase. we'll make a discussion for the effect of pressure on the electronic and magnetic properties of the compound $Mn_(2)FeSn$ for that type structure.

We had carried the calculations out using the $CASTEP$ code[33], which is a method implementation based on plane wave method coupled with the pseudo-potential approximation within the framework of the density functional theory (DFT). To determine the potential for exchange and correlation, we used the $GGA - PBEsol$ approximation[170].

4.1 Calculation parameters

The calculations were performed in the framework of the density functional theory (DFT) First-principle (Hohenberg and Kohn 1964; Kohn and Sham 1965) using Generalized gradient approximations (GGA) and Perdew- Burke- Ernzerhof (PBEsol)[171, 172, 173] for solids besides the spin-polarized feature.

We used the software program $CASTEP$ code which is based on pseudo-potential approximation and plane waves method, in order to determine the different physical properties structural, electronic and magnetic.

To treat the electron-ion interaction, we have chosen for each element, an ultra-soft pseudo-potential from Vanderbilt[166], which is used to reduces the cut-off energy.

To define the most stable structure, we calculate the total energy for the different structural types of Mn_2FeSn in equivalent site occupations with XA type structure crystallisation, with

Wycoft positions[174].

The states valence considered during our calculations are:

Mn : $3d^5 4s^2$

Fe : $3d^6 4s^2$

Sn : $5s^2 5p^2$

The d layer characterizes the transitional metals Mn and Fe ,and Sn is from the poor metals an SP element.

In this work, we have used the same parameters, cut-off energy and the number of k-points for the studied types system. The convergence tests that we carried out led us to choose cutoff energy of 380 eV for our compound,a selection of the *Brillouin* zone was carried out with a $(8 * 8 * 8)$ k points grid.

With regard to electronic properties, the band structures have been calculated following the path: W -L - G - X -W -K, it is formed by five points high symmetry in the Brillouin zone. The converge parameters (the convergence tolerance) for this optimization are set as follows: the energy change per atom is less than 10^{-6} (eV/atom), the maximum forces on atoms are less than 0,03 ($eV/A°$), all the stress components are less than 0,05 (GPa), a maximum displacement less than 10^{-3} ($A°$) and with the BFGS algorithm Broyden-Fletcher-Goldfarb-Shanno (BFGS) minimization[175, 176].

4.2 Structural properties of compounds

4.2.1 Crystal structure

The inverse Heusler compounds characterize with the atomic number of X that is smaller than that of Y which implies that the electronegativity of Y is greater than X. Here, the Heusler-like inverse structure Hg_2CuTi with the space group $F\bar{4}3m$ (216) is observed with the X atoms are placed in Wyckoff positions 4a (0,0,0) , and 4c (1/4, 1/4, 1/4), Y and Z in 4b (1/2, 1/2, 1/2) and 4d (3/4, 3/4, 3/4), respectively. The inverse Heusler compounds crystallize in the so-called XA or X_α structure,where the sequence of the atoms is X-X-Y-Z with Hg_2TiCu prototype[12].

We used an experimental lattice parameter of Mn_2FeSn compound equal to $6A°$ [17, 177], for the three types of structures. By changing positions, three types of occupations arrangement are possible[178, 76].

We had calculated the final energy for the three types of structures (group $F\bar{4}3m$ (Space group no. 216)), in order to find the site occupancy for the most stable structure.The proposed occupancies reported in the table (see figure 4.1)[4].

Based on the results that we got from the geometric optimization (see figure 4.2), we have drawn the energy plots versus the pressure applied and the volume for the three types of the conventional cell in order to find the most stable combination (see figure 4.5).

It was shown, from the results, that the second type is the most stable one with the smallest energy value, besides the occupations for the different lattice sites are 4c (1/4,1/4,1/4), and 4d (3/4, 3/4, 3/4) for the double Mn ,and 4a (0,0,0), 4b (1/2,1/2,1/2) for Sn and Fe respectively .

	4a(0,0,0)	4c(1/,1/41/4)	4b(1/2,1/2,1/2)	4d(3/4,3/4,3/4)
Type 1	Sn	Fe	Mn	Mn
Type 2	Sn	Mn	Fe	Mn
Type 3	Mn	Fe	Sn	Mn

Figure 4.1: different site occupations for the three types with atoms on Wycoft position [4]

	Conventional cell			Primitive cell		
Configurations	a_{Exp} (A°)	a_{Cal} (A°)	E_{Min} (eV)	a_{Exp}(A°)	a_{Cal}(A°)	E_{Min}(eV)
Type 1	6	6.0918	-9020.6407	6	4.3065	-2255.1662
Type 2	6	6.1037	-9021.3588	6	4.3154	-2255.3517
Type 3	6	6.09118	-9020.6407	6	4.3051	-2255.1680

Figure 4.2: Schematic represent lattice parameter experimental and theoretical, the final minimum energies values for the three different configurations for the primitive and conventional cell

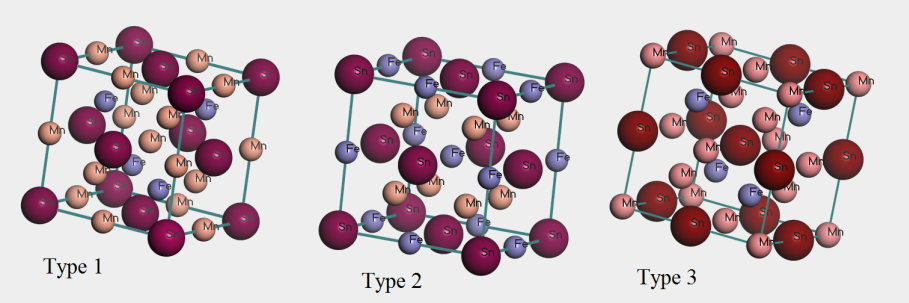


Figure 4.3: Schematic representation of Mn_2FeSn inverse Heusler site occupancies structures

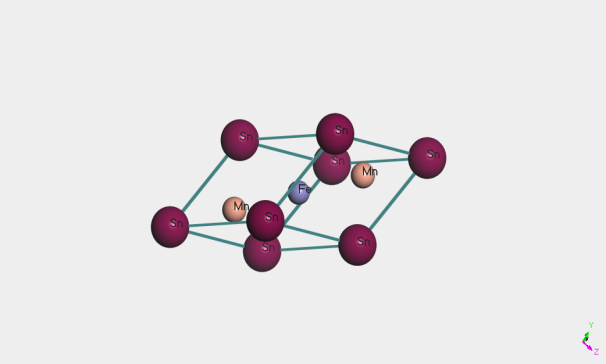


Figure 4.4: Schematic representation of Mn_2FeSn inverse Heusler primitive cell.the preferred occupations for the different lattice sites are 4c (1/4,1/4,1/4), and 4d (3/4, 3/4, 3/4) for the double Mn ,and 4a (0,0,0), 4b (1/2,1/2,1/2) for Sn and Fe respectively

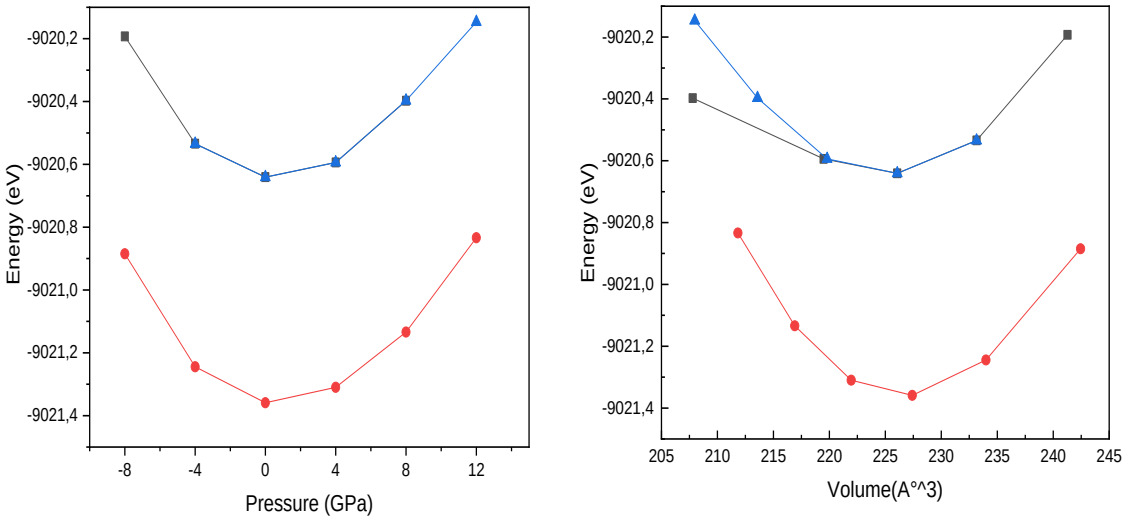


Figure 4.5: Schematic represent the variation of the total energy as a function of the pressure applied and the volume for the three different configurations for the conventional cell.

The conventional cell contains eight atoms inside of it structure (see figure 4.3 type two structure) and the figure 4.4 represent it primitive cell.

4.2.2 Equilibrium state and Pressure effect

In this section, we determined the parameters in the equilibrium state (P = 0 GPa , T = 0 K): the final minimum energy E_0 , cell volume, and the bulk modulus of compressibility B.

We started with the Geometry Optimization task that allows us to refine the geometry of a 3D periodic system to get a stable structure. We did that by performing an iterative process with adjusting the space group, the coordinates of atoms, and the cell parameter,then we supposed that the compound has spin-polarization character, we fixed the energy cut-off and Monkhorst pack grid[150] as mentioned above, and we choose the ultra-soft pseudo-potential for the reciprocal space.

Hence, we studied the effect of hydrostatic pressure from -12 to 12 GPa on the lattice parameter and cell volume, so that the total energy of the structure is minimized.

1. **equilibrium state**

   In this subsection, we plotted energy curves as a function of the volume for the primitive and conventional cell of the stable structure, using Origin program software. By fitting the calculated energy versus volume using the proper form of the equation of state, to gets the theoretical equilibrium unit cell volume V_0 and some other properties, such as the isothermal bulk modulus and its first derivative regarding pressure[179, 180] which is given by the following equation :

$$E(v) = E_0 - \frac{V_0 B}{B' - 1} + \frac{BV}{B'}[\frac{[\frac{V0}{V}]B'}{B' - 1} + 1] \tag{4.1}$$

   Where E_0 is the minimum energy, V_0 is the volume at equilibrium (P = 0 GPa), B is the Bulk modulus of compression, and B' is its derivative regarding the pressure. The compression modulus of a material defined as the resistance of the matter versus changes in volume; i.e. the ratio of the applied stress when that material is being compressed[181, 182].The relation between volume and pressure is given by :

$$V = V_0 + [1 + \frac{B'P}{B}]^{\frac{1}{B}} \tag{4.2}$$

   The Bulk modulus of compressibility determined by:

$$B = V\frac{\partial^2 E}{\partial V^2} \tag{4.3}$$

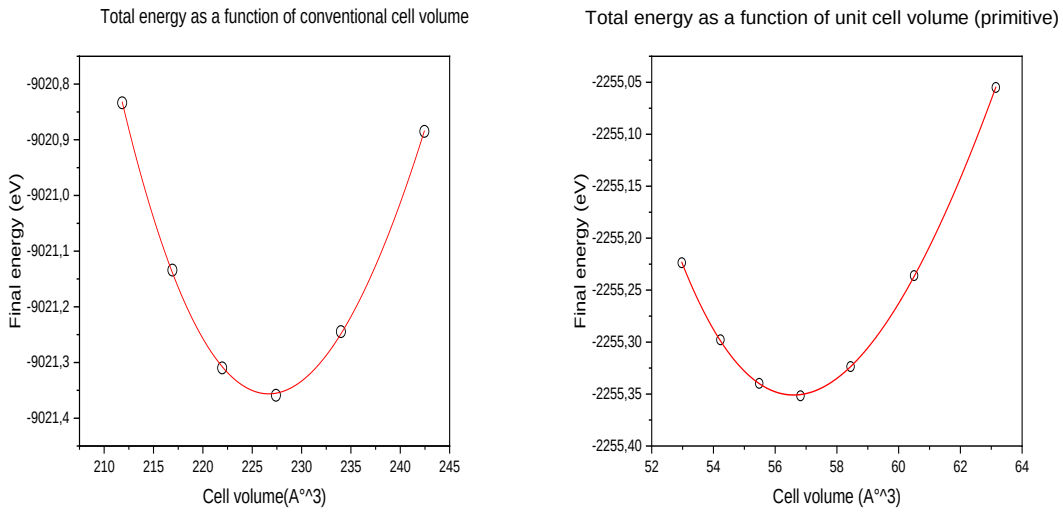


Figure 4.6: Total energy evolution as a function of the volume for the primitive and conventional cells

	Conventional cell			Primitive cell		
	B (GPa)	E_{Min} (eV)	V_0 (A^3)	B(GPa)	E_{Min} (eV)	V_0 (A^3)
Castep Results	274.37	-9021.3588	227.403	227.92	-2255.3517	56.821
EOS Fit Results	154.12	-9021.3562	226.671	154.58	-2255.350	56.596

Figure 4.7: Quantities values that obtained in the equilibrium state

The variation of the total energy as a function of the volume for the primitive and conventional cell is shown in Figure 4.6. The volume V_0 and the energy E_0 at equilibrium determined by the minimum of the Total energy curve .

The solid line (in red) represents the theoretical fit by Murnaghans equation of state over the drop lines that represents the origin curve. There is no experimental information available to compare the results obtained, so we made a comparison between primitive and conventional cells to get more accurate information about the compound .

The DFT calculation agrees with Murnaghans rule in the results of the two cells , except in the values of the bulk modulus of compressibility which is the only discrepancy between the DFT data and experimental data.

2. **Pressure effect on lattice parameter and cell volume**

Hydrostatic pressure is the quantity that defined as force per unit volume where the force

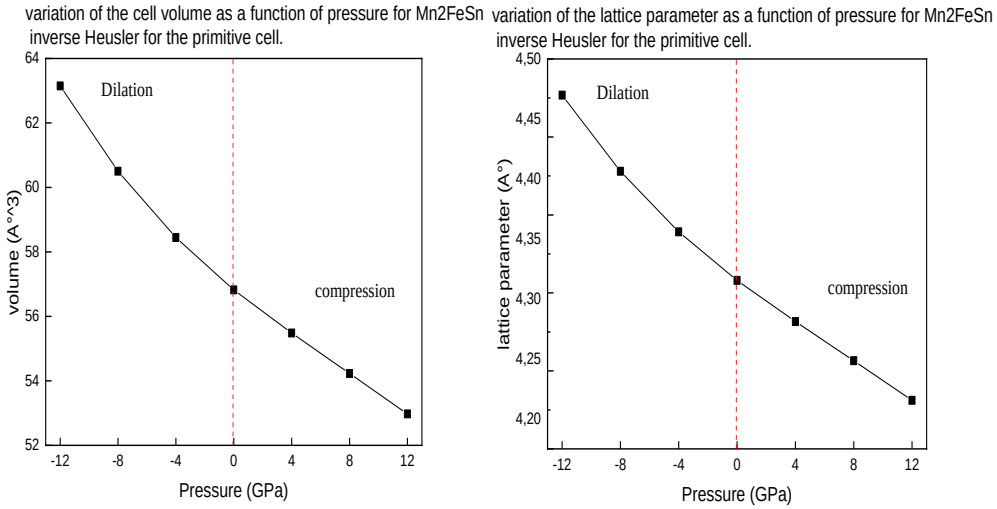


Figure 4.8: Pressure effect on lattice parameter and cell volume for the primitive cell

acts in selected directions to the surface.It is one of the most elementary notions encountered in the fields of naval architecture and marine engineering.. etc, besides, it allows to affect the physical properties shape and structure of volume (dilation, distortion, compression), essentially influence the material behaviour and it properties[183, 184].

Wherefore, we applied an external stress (hydrostatic pressure) from -12 to 12 (GPa) and calculating the variations on the structural parameters of the compound by the geometry optimization. We observe in the figure 4.8 a decline in volume and lattice parameter values versus an increase in pressure. Hense, the negative pressures reflect a dilation effect and the positive one a compression effect.

4.3 Electronic properties of compounds

4.3.1 Brillouin zone

The Brillouin zone is defined as the Wigner Seitz primitive cell of the reciprocal lattice. In solid-state physics, the Brillouin zone is defined as the Wigner Seitz primitive cell of the reciprocal lattice[185]. Although the terms "Wigner-Seitz cell" and "first Brillouin zone" refer to identical geometrical constructions to the primitive cell, in practice Brillouin zone term applied only to the K-Space cell[186, 187, 147].

In periodic systems. The energy of a band varies as a function of K. The energy minima and maxima of each band are generally found on the points and axes of high symmetry of the reciprocal lattice[188, 189].

The band structures have been calculated according to special lines that connecting the mentioned points K of high symmetry in the Brillouin zone for the cubic lattice have the following

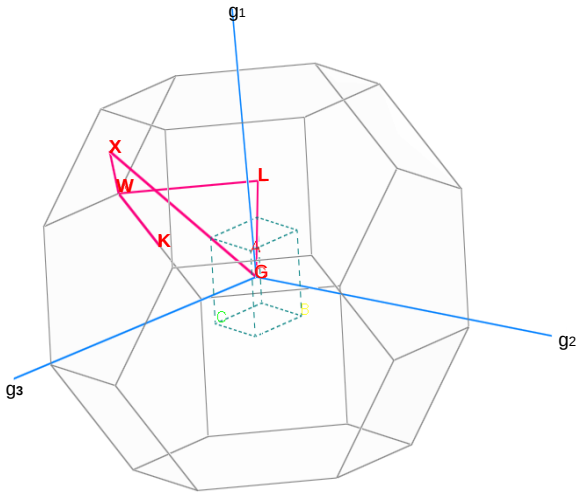


Figure 4.9: The first Brillouin zone for the Mn_2FeSn FCC lattice.g 1, g 2, g 3 are the reciprocal base vectors

coordinates: W (0.5, 0.25, 0.75); L (0.5, 0.5, 0.5); Γ (0, 0, 0); X (0.5, 0, 0.5); W (0.5, 0.25, 0.75) and K (0.375, 0.375, 0.75) (the point Γ is the center of the ZB, noted as the point G in the figure 4.9). Where the irreducible part encased by red lines is the path that we'll use to draw the band structures in the next section.

4.3.2 Band structure

The band structure allows us to visualize the energy occupation of electrons in the crystal, hence subtending with great precision the allowed energy bands diagrams, therefore determine the nature of the material studied (insulator, conductor, semiconductor) of our compound.

The valence (V_B) and conduction (C_B) bands formed by packets of several bands known as energy levels or atomic levels, that separated by a certain amount of energy known as band gap or the forbidden energy gap[190].

The dispersion of the electronic bands give the energies of an electron as a function of the wave vector k, represented in reciprocal space, following only the directions of high symmetry in the first Brillouin zone. The strong hybridization between the d-states of the transition metal atoms is responsible for the gap[98].

The calculated band structures at along with the high symmetry points in the Brillouin zone for the Mn_2FeSn compound for two different pressure 0 and -4 GPa are shown in figure 4.10.

In this figure, we notice that there is an overlap in the majority band structure (spin up band), this reveals a metallic characteristic. On the other side, the minority band structure exhibits a semiconducting behaviour, with an indirect energy gap along the axis of high symmetry X in the conduction band and W in the valence band for the two different pressure.

So then we are going to make a discussion in the next part only with the band that contains

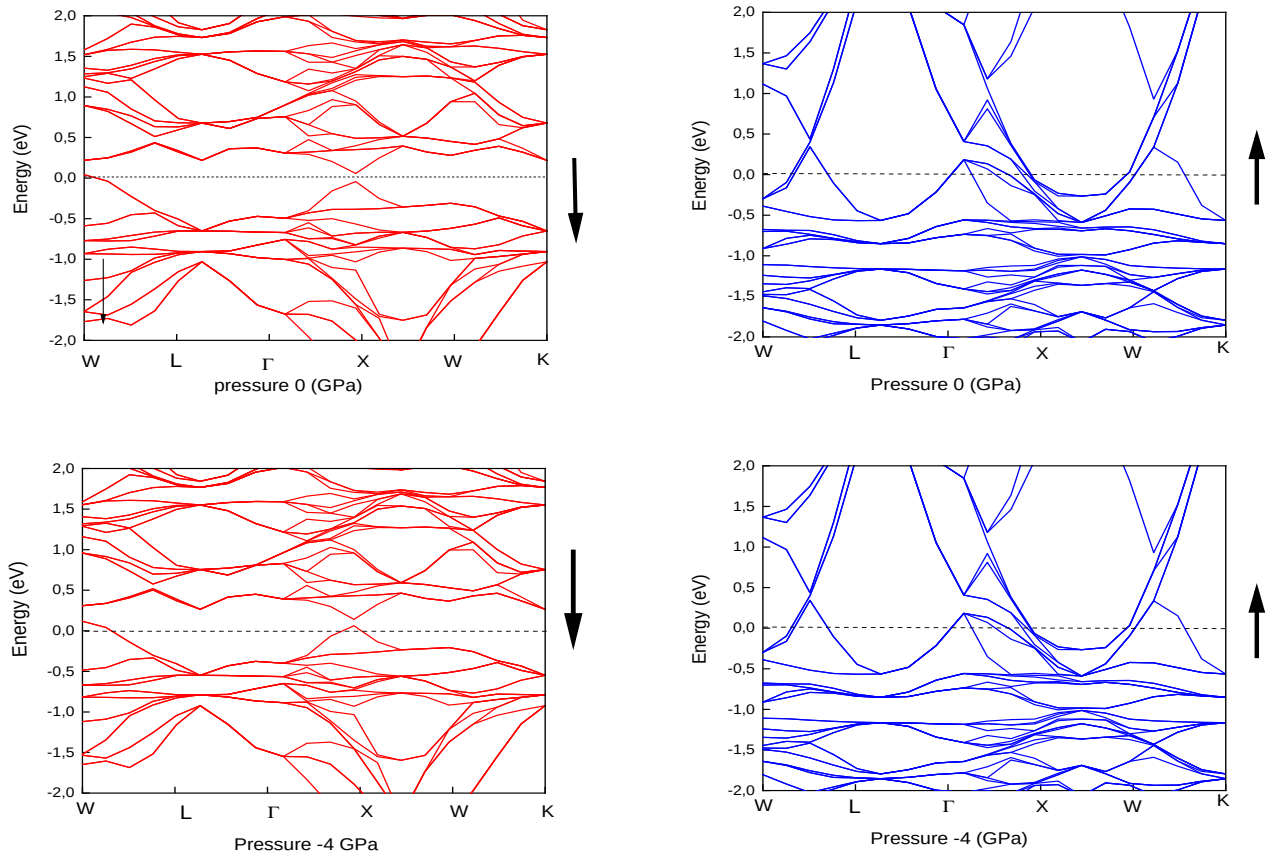


Figure 4.10: Schematic representation the band structures of 0 and -4 GPa for majority and minority spin.

gap energy which is in the minority band structures (spin-down band). The bands structures of Mn_2FeSn give information about the half metallic character for this material compound[191, 192, 193, 90].

Then, using the optimized structures under the effect of different pressure from -12 to 12 GPa, and following the path in the reciprocal space : W - L - Γ - X - W - K , we plotted the spectra of the minority band structures for the compound Mn_2FeSn (see figure 4.11 and 4.12).

For pressure values ranging from 0 to 12 Gpa, there is a displacement from the bottom of the conduction band towards energies lower on the top of the valence band.This has leads to an increase in the band gap width for minority spin states.

The bottom of the conduction band decreased until it touched the Fermi level[194] (E_F) in the value of 2 GPa ($E_g = 0.11026eV$) , and shows the case of a gapless Half metallic[9] (see Fig 2.6(c)); while it exceeded the Fermi level at pressure value from 4 up to 12 Gpa, it shows the metallic behaviour.

The top of the valence band increases to touch the Fermi level (E_F) and exhibit other case of gapless half metallic at a hydrostatic pressure value -2 GPa ($E_g = 0.0793eV$) , while it moves

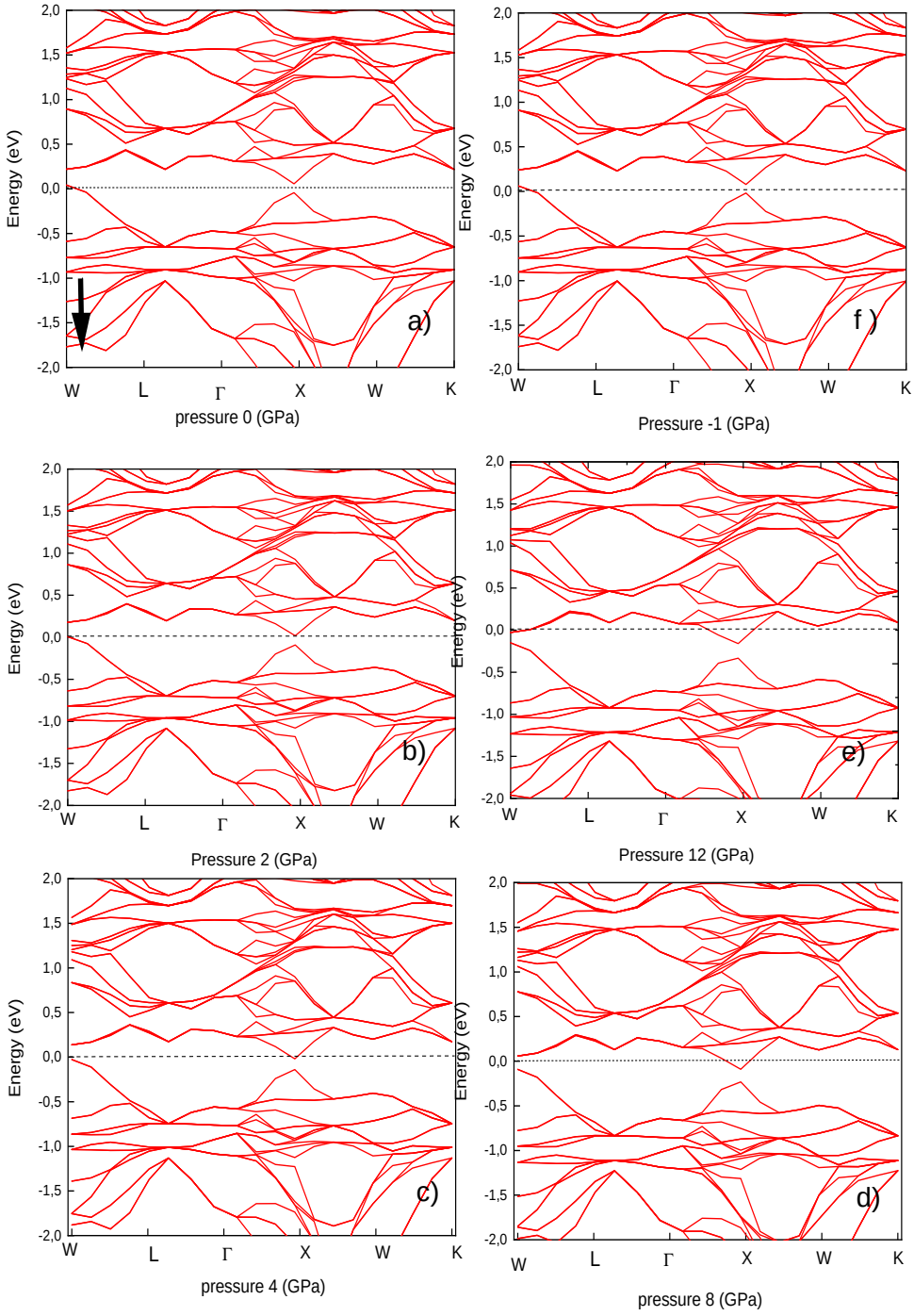


Figure 4.11: Schematic representation of the band structure for minority spin under different pressure(0, 2, 4, 8, 12, -1 GPa).

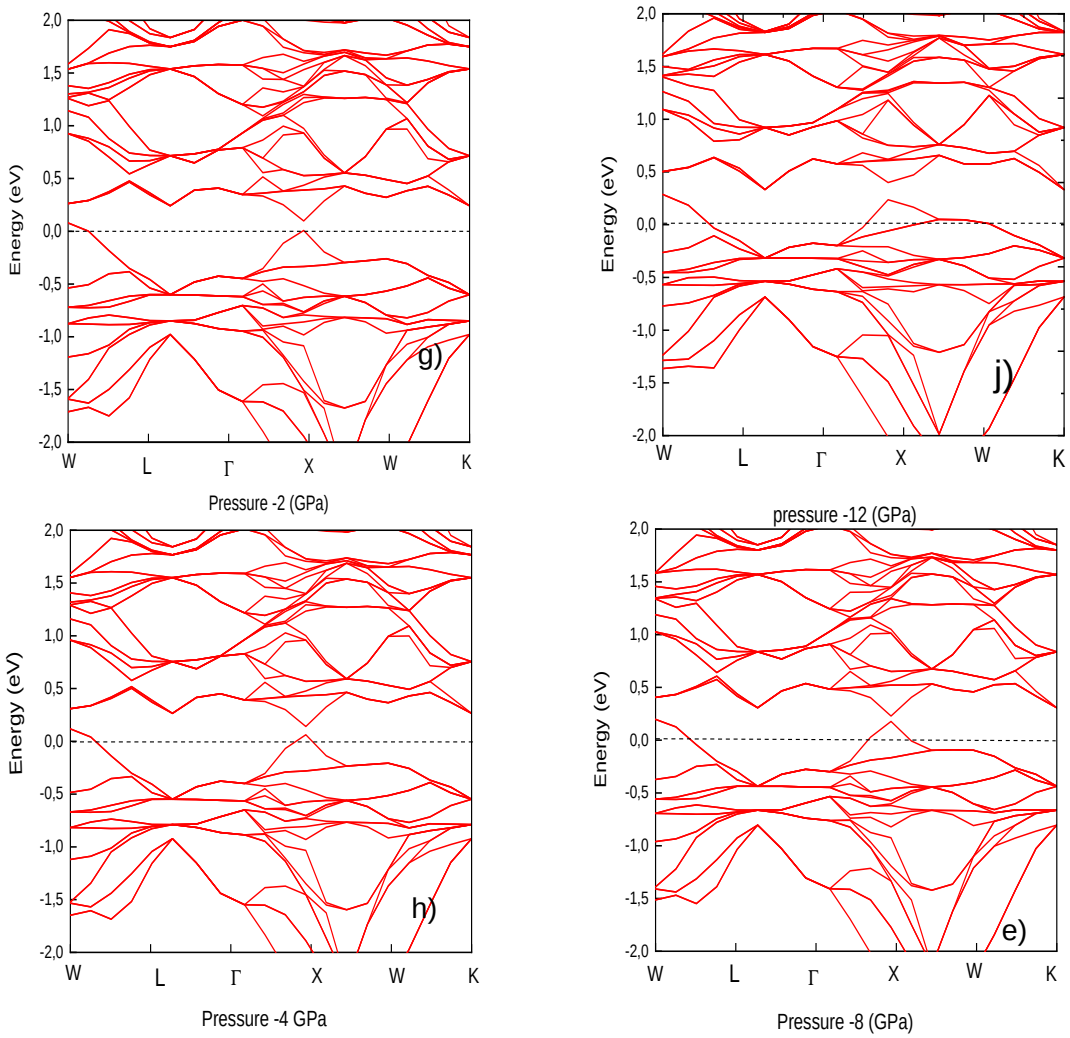


Figure 4.12: Schematic representation of the band structure for minority spin under different pressure (-2, -4, -8, -12 GPa).

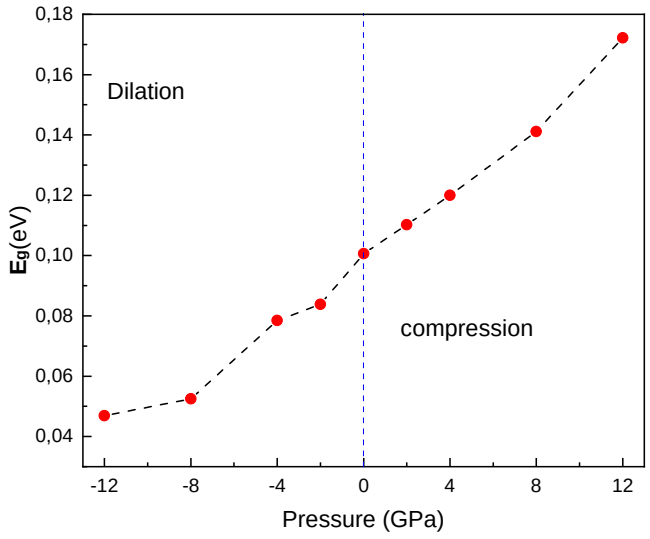


Figure 4.13: Pressure effect on the forbidden band

towards the bottom of the conduction band and exceeding the Fermi level (E_F) ; thus inducing a reduction in the forbidden band in addition to the appearance of the metallic behaviour from -4 to -12 GPa .

As result , Under the application of a certain pressure, the material changes its behaviour from half-metallic semiconductor with indirect gap that can be seen through the deference in the energy along the axis of high symmetry X in the conduction band and W in the valence band from 1 to -1 GPa and gapless half metallic for 2 and -2 GPa ; to the metallic behaviour from 4 to 12 and -4 to -12 GPa.

4.3.3 pressure effect on the energy gap

We mentioned that there is a band gap If an energy gap exists in the band structure of a material. The physical properties of insulators semiconductors and metals can be determined to a large extent by their band gaps, and control their electronic properties[147, 195].

The curve in figure 4.13 clarify the variation of the gap energy of the material Mn_2FeSn as a function of the hydrostatic pressure. We note that there is an increase in the gap's and the pressure values together, which mean that there is a direct proportion between the two quantities, for the compression and expansion phases.

As info, the GGA approximation underestimates the energy gap, that's why we get values miner 0.2 (eV)[196, 197]. So we proved that the hydrostatic pressure significantly affects the values of the gap energies of materials .

4.3.4 Densities of states (TDOS,PDOS)

After determining the optimized parameters of the ground state using the GGA PBEsol functional , we will study the electronic behaviour of the compound. The electronic density of the state is one of the important properties that give us information about the behaviour and character of the compound.

To determine the origin of the orbital contributing to the formation of the different parts of the spectra of the Mn_2FeSn electronic band structures, we calculated the total (TDOS) and partial (PDOS) electronic density of states shown in figure 4.14.

It is clear from the figure that The compound has a magnetic character due to the asymmetry between the majority and minority spin density of states. The peak in the majority spin state gave the material a strong polarization at the Fermi level for 0 GPa the polarisation is (57%) and for 12 GPa is (79%).

The band gap of Mn2FeSn has been determined mainly by the bonding and anti-bonding states created from the hybridizations of the states d between the couple Mn-Mn and the atom Fe[186].

The valence band of Mn_2FeSn comprises splitting parts: a part with a small contribution in the energy range between (-10 to -8 eV) and (-8 to -4 eV) formed by the 5s and 5p state respectively of the element Sn (Sn-s and Sn-p), then, the second part located between the Fermi level from -4 to 4 eV in the conduction band formed by the mixture of the 3d states of double Mn and Fe transition elements (Mn-d) (Fe-d). Than The lower part of the conduction band results at most from the 5p and 5s states of Si element. Thus indicating that the 3d state of double atoms Mn and Fe are the most dominant states[198].

4.4 Magnetic properties of compounds

4.4.1 Magnetic moment

The total magnetic moment and magnetic moment of Heusler compound atoms Mn Fe Sn under pressure from -12 to 12 GPa are estimated from the electronic population analysis of Mulliken[199], calculated and plotted in Figure 4.15 . The magnetic moments of the double Mn atoms are always positive and decrease from -12 to 12 GPa, besides the increase in Sn magnetic moment with negative tiny values.

From the different variation effects of Atomic magnetic moments of all atoms, the total magnetic moment is almost equal to an integer value of 2 μB through the entire pressure range. On another side, for the inverse Heusler alloys, the total magnetic moment follows the Slater-Pauling rule[5]:

$$M_t = N_v - 24\mu B \tag{4.4}$$

Where N_v is the accumulated number of valence electrons in the primitive cell[82, 88].

The Mn_2FeSn compound has 26 valence electrons($Mn : 3d^5\ 4s^2$, $Fe : 3d^6\ 4s^2$, $Sn : 5s^2\ 5p^2$) Using the Slater-Pauling rule, its total magnetic moment corresponding is 2 μB. This value agrees with the summation calculated magnetic moment of the atomic magnetic moments besides the

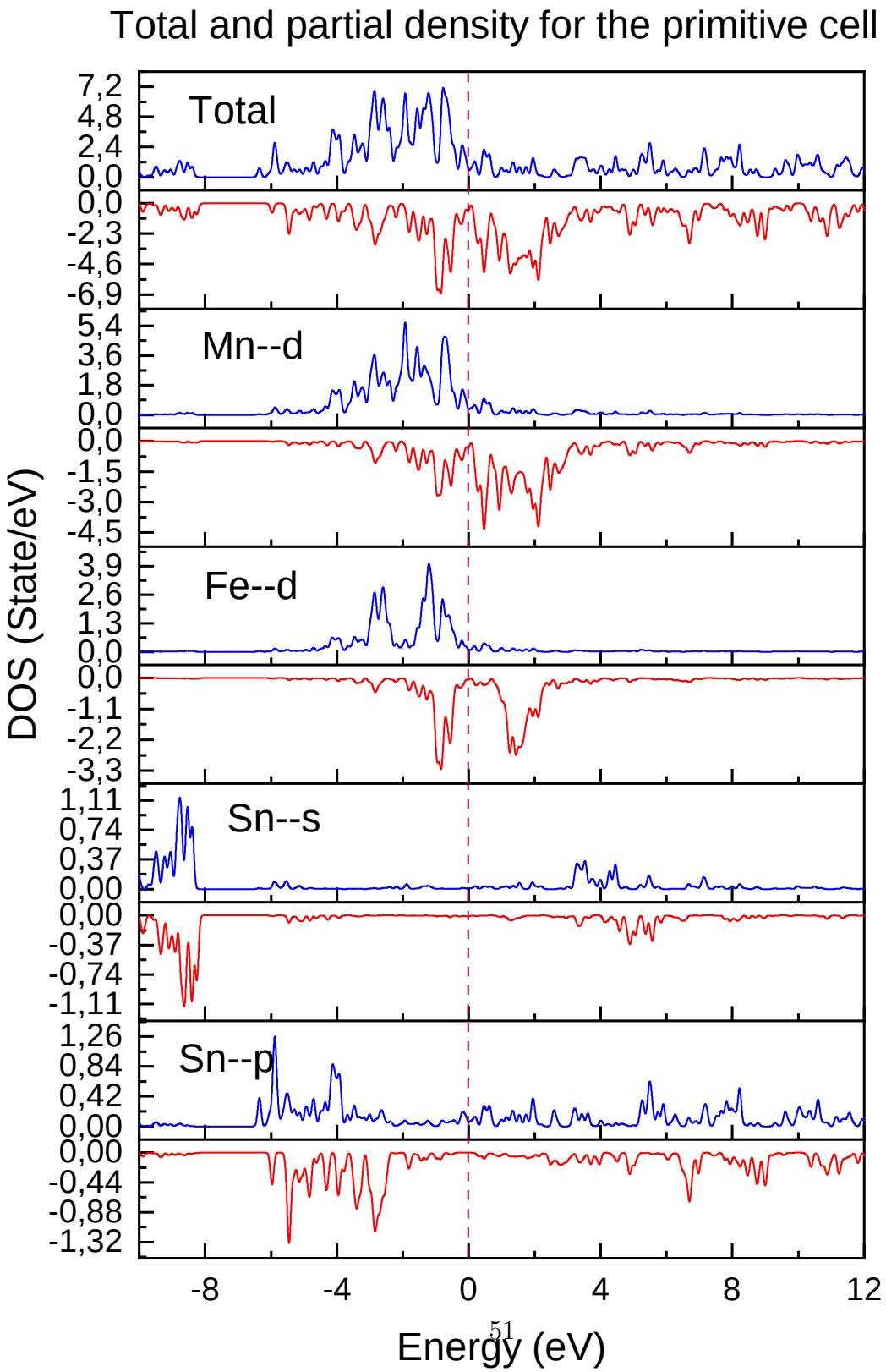


Figure 4.14: Calculated spin-projected total and partial DOS plots for Mn_2FeSn at 0 GPa.

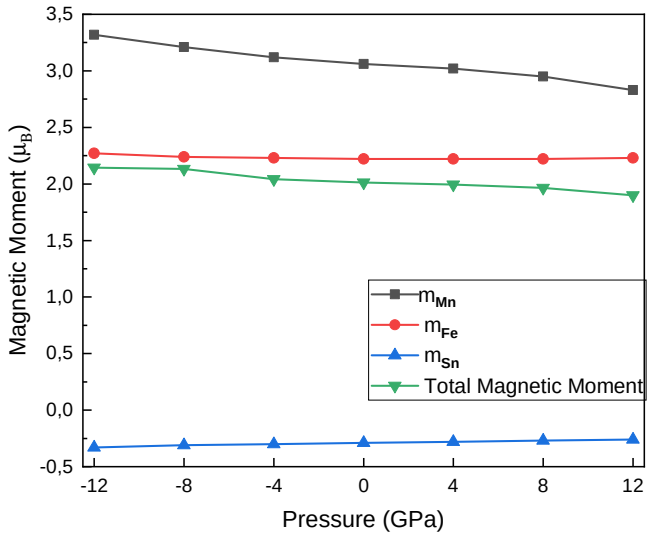


Figure 4.15: Total and partial magnetic moment as a function of pressure.

results in literatures[200]. The behaviour of the total magnetic moment characterizes the Heusler compound[176, 201].

4.4.2 Pressure effect on Magnetic moment

In the figure 4.15, we observe that the magnetic moment's evolution versus The pressure; the major contribution in the M_{total} comes from the Mn and Fe atoms.

Whereas the pressure variation has a weak effect on the Total magnetic moments, that's because of the strong resistance of the materials to change the volume.

Moreover, we observe that the Partial magnetic moments of Fe and Sn changed with a weak variation, while the partial magnetic moments of Mn decreased versus the pressure increasing.

The application of hydrostatic pressure changes the hybridization between d orbital neighbouring atoms with changes in the atomic distance character, a Well-known behaviour in most Heusler alloys as Jahn Taller distortion[202, 203, 204].

4.4.3 Spin polarization

Spin polarization is an important quantity in spintronic feild, it measures the asymmetry between the two confining spin states.

The polarization at the Fermi level (E_F) help to understand the asymmetry between the densities of spin up and spin down states, that represented the operation is done by the following

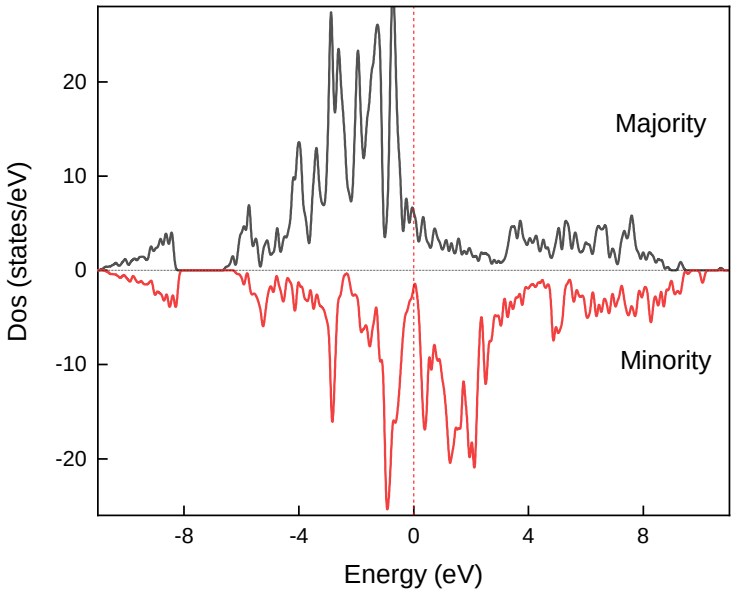


Figure 4.16: Calculated spin-projected total DOS at 0 GPa for the inverse Heusler Mn_2FeSn.

relation:

$$P = \frac{\rho\uparrow(E_F) - \rho\downarrow(E_F)}{\rho\uparrow(E_F) + \rho\downarrow(E_F)} \tag{4.5}$$

For better results, we changed the staining width to 0.02 and the number of points per eV to 300 (see figure 4.16).The results change according to the pressure values applied on it, the convergence tolerance, the quality of calculation...

The figure 4.17 shows the total density of the inverse Heusler Mn_2FeSn states, calculated using method based on density functional theory, at 99% of the polarization value taken from the Open Quantum Materials Database (OQMD) website[17] .

Whereas , from our calculations we obtained percentage values from 40 to 80% , its evolution versus the hydrostatic pressure of a conventional cell shown in the figure 4.18. In the compression part, we notice that the polarization decreases from -12 GPa which corresponds to (68%) to -4 GPa (42%), in the same part from -4to 0 GPa (56%), the plot increases.

When the pressure exceeds 0 GPa in the compression part, the polarization keeps increasing linearly and reaches its maximum value of 79% .

Due to the lower density value at the Fermi level (E_F) for the minority spin electrons (compared to the DOS values at E_F for the spin majority electrons), it gives a important spin polarization at the Fermi level .

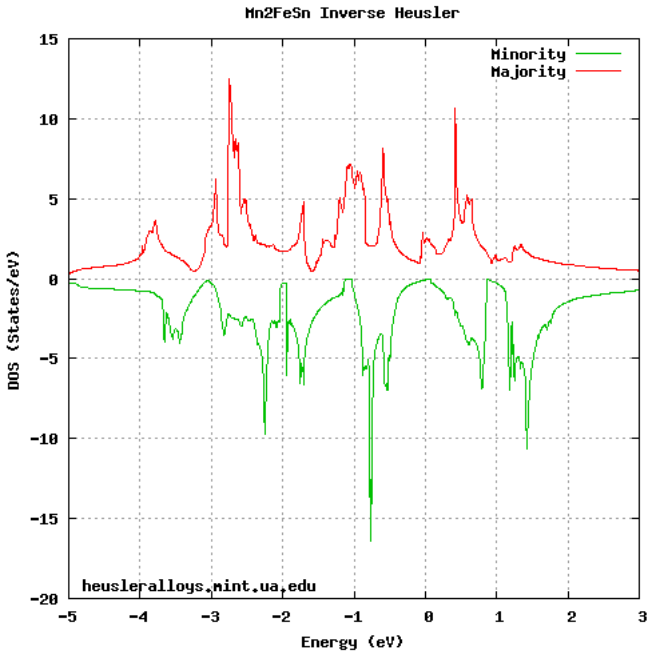


Figure 4.17: Calculated spin-projected total DOS Mn_2FeSn[17].

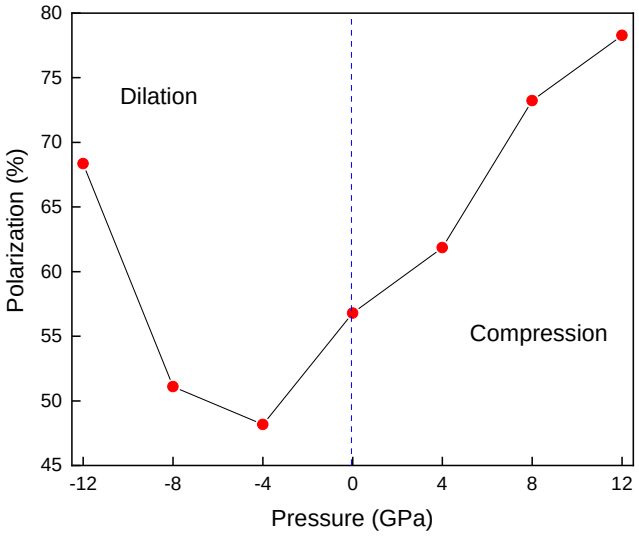


Figure 4.18: Percentage polarization values versus pressure.

Conclusion

In this, master thesis, we have made a study of the electronic and magnetic structural properties of the Heusler-type compound, that was carried within the framework of density functional theory (DFT), by the use of the CASTEP code, which is based on the pseudo-potential and plana wave (PP-PW) method.

The effect of the exchange and correlation has been processed under the GGA-PBEsol approximation for the two spins states (up and down). The results got from the study can be summarized:

- Structural properties: First, we had determinate that the compound is an inverse Heusler based Mn2 with the atomic number of Y is higher than that of X, thus the compounds crystallize in the so-called XA or X_α with (group $F\bar{4}3m$ and (Space group no. 216))[76].

  Then, Considering the three types of occupations arrangement, the geometrical optimization allowed us to conclude that the most stable combination of the Mn_2FeSn is the type two structure which preferred the occupations of sites with 4c (1/4,1/4,1/4), and 4d (3/4, 3/4, 3/4) for the double Mn (x), and 4a (0,0,0), 4b (1/2,1/2,1/2) for Sn(z) and Fe(y) respectively.

  The inverse Heusler Mn_2FeSn type two structure is perchance identical to the regular Heusler X2YZ that crystallize with $L2_1$ structure with (group $Fm\bar{3}m$ (space group no. 225) symmetry),where the Wyckoff positions is 4a (0, 0,0)(z) , 4b (1/2, 1/2, 1/2)(x) , and 8c (1/4,1/4, 1/4)(x)[87] .

  Quantities at equilibrium states such as V_0, B, and E_{min} from the equation of state fit are good in agreement with the Castep code software results . The bulk modulus B exceeds 274 GPa, which indicates that the Mn_2FeSn exhibit high resistance against the volume changes under external stress 0 GPa[182].

- Electronic Properties:

  Electronic structure analysis shows that this material is ferromagnetic, with spin polarizations of (57%) at 0 GPa at the Fermi level.

  We noted that there is an overlap in all majority bands structures (spin up bands), which reveals a metallic behaviour, besides a half metallic semiconductor character between 1 to -1

GPa, metallic character in most minority bands structures, besides to gapless half metallic behaviour under 2 and -2 GPa hydrostatic pressure.

TDOS and PDOS analysis indicate strong hybridization between the d orbitals for Mn-Fe and Mn atoms, which results in energy gaps for the minority spin state.

- Magnetic Properties:

  The total magnetic moment M_{tot} of Mn_2FeSn obtained from castep is in good agreement with the Slater–Pauling rule and the result from literature[200]. We considered that the M_{tot} is mainly caused by the magnetic moment of the Mn and Fe atoms.

  The half metallicity of the compound was analysed and proved by calculating the polarization P . We obtained a maximum value of polarization P=(78%) at hydrostatic pressure 12 GPa , we can get better results for the polarization by increasing the pressure, and maintained it at large pressure values.

Finally, the gapless half-metallic and half metallic semiconductor behaviours made the compound a perspective candidate For future applications in Spintronics.

Appendix A

Fundamental notions associated with the CASTEP code use

A.1 The CASTEP code

CASTEP (Cambridge Serial Total Energy Package Program)[33], is a code uses first principles density functional theory,in order to simulate a wide range of materials including crystallized solids, surfaces, particles, liquids, and amorphous materials.

It allows calculating the properties of any substance that can be considered as a group of nuclei and electrons with The only restraint is the limited speed and memory of the computers being used.

In 1986, Mike Payne[155] wrote the first version of CASTEP, then it took him two months to produce a fully functioning program.

This code provides information on the total energies, forces, and stresses applied on the atomic system, as well as calculating the geometric optimisation , electronic structure, band structures, optical spectra and elastic constants. This program was developed by Professor K.C. payne and marketed by Accelerys.

This program is based on quantum mechanics and the calculations are performed using the pseudo-potential coupled with the plane wave technique (PP-PW) by solving the Kohn-Sham equation 3.34 within the framework of density functional theory (DFT).

This code is used to simulate the total energy by special integration of the K points in the first Brillouin zone with the plane wave base by the Monkhorst and Pack method.

CASTEP is able to improve the atomic geometry of the system in many different ways. The most widely used is BFGS[205], which is an iterative method for solving single particle nonlinear optimization problems[206].

The aim of the simulations is not to use experimental (empirical) data but to rely only on quantum mechanics, and that is what made the approach very ambitious given its advantages of reducing the cost of experiments and operations besides computer resources and saving time.

It was originally developed by Payne and co-workers in the late 1980's and early 1990's[207,

208, 33].

A.2 Geometric optimization

CASTEP allows the optimization of the structure by reducing its energy under the name of geometric optimization.

The location of the atoms around their initial occupancies is modified by applying the new calculated energy, several times until a constant affinity threshold is reached, i.e. determining the electronic ground state of the studied systems (SCF), reducing the energies that apply on each atom .

This is done by implementing one of the SCF (Self-Consistent Field) algorithms in the CASTEP code.

The geometric optimization is often at the equilibrium point (P = 0GPa, T = 0K) which is the first step in simulation.

One of the advantages of CASTEP is that it improves the cell in the presence of external stress such as hydrostatic pressure[209, 210].

A.3 Electronic band structure

In solid-state physics, the range of energy levels of a solid contains electrons within it (the electrons occupy the energy levels, it is distributed according to Pauli exclusion principle), it is described by the electronic band structure.

It provides electronic levels in crystal structure which are characterized by a Bloch vector k and a band index n.

Then, it well has widely known that the properties of any materials depend principally on their electronic energy-band structures, especially on such band parameters as the energy gaps, the position of the band edges in the Brillouin zone.

In addition, through these electronic band structures it can determine the character of materials; metal, semi-metal, semi-conductor, and insulator, through the energy gap.

the electronic band structure of solids describes the quantum-mechanical behaviour of electrons and reveals the eigenvalues associated with conduction and valence bands in specific directions in the Brillouin zone of a crystal.

The electrons possess only certain discrete energies, which can be depicted in an energy-level diagram as a series of distinct lines.

The electrons that contribute to the electrical conduction occupy the higher energy bands that correspond to the valence band. The valence band can be fully or partially occupied. The conduction band is the lowest energetic band with unoccupied states. [211, 212, 213, 214]

A.4 Density of state

Since the band structure can be used to calculate the total energy of the solid, from which one can determine a wide variety of thermodynamic, mechanical properties and the possible optical excitations which in turn determine the colour, reflectivity, and dielectric response of the solid.

Otherwise, it has been considered that the density of states as a function of the energy, is a beneficial concept in analyzing the band structure of solids.

The Density of States (DOS) of a system can be defined as the number of states per interval of energy at each energy level that is available to be occupied by electrons.

Where the density of states per unit volume is defined as:

$$g(E) = \int \frac{d\vec{k}}{(2\pi)^d} \delta(E - E(\vec{k})) \tag{A.1}$$

d is the dimension, k is the wave vector, E is the energy per unit volume[215].

For a system, a high DOS at a specific energy level means that there are many states available for occupation and zero DOS means that no state can be occupied at that energy level.

PDOS are based on the analysis of Mulliken populations and carried out by projecting mono-electronic orbitals on the basis of atomic orbitals located around the different nuclei of the cell[216, 217, 214, 218].

A.5 The atomic population of Mulliken

As a consequence of the applied concepts transfer charge and atomic charge, that continue to play an important role in quantum chemistry and much research continues to being done to refine the concept of an atomic charge.

Mulliken's formalism was proposed in 1955 which describe the atomic populations, its consider as commonly used technique for electronic structure calculations, that mainly based on first-order density functions within a LCAO MO theory approach[199].

Later, many alternative definitions of atomic charges and populations have been presented as a natural consequence of the previous statements 1966 Nobel Prize motivation: "for Mulliken fundamental work concerning chemical bonds and the electronic structure of molecules by the molecular orbital method".

Finally, the population analysis in CASTEP is performed using a projection of the PW states onto a localized basis using a technique described by Sanchez-Portal[219] et al. in 1995[218, 220, 221].

Bibliography

[1] Kong, L.B., Liu, L., Yang, Z., Li, S., Zhang, T., Wang, C.: Theory of ferrimagnetism and ferrimagnetic metal oxides. In: Magnetic, Ferroelectric, and Multiferroic Metal Oxides. Elsevier (2018) 287–311

[2] Zhang, S., Zhao, D.: Advances in magnetic materials: processing, properties, and performance. CRC press (2017)

[3] Sagnotti, L.: Magnetic Anisotropy. In Gupta, H.K., ed.: Encyclopedia of Solid Earth Geophysics. Springer Netherlands, Dordrecht (2011) 717–729

[4] Graf, T., Felser, C., Parkin, S.S.: Simple rules for the understanding of heusler compounds. Progress in solid state chemistry **39**(1) (2011) 1–50

[5] Galanakis, I.: Theory of heusler and full-heusler compounds. In: Heusler Alloys. Springer (2016) 3–36

[6] Alijani Zamani, V.: Structure and properties of quaternary and tetragonal Heusler compounds for spintronics and spin transfer torque applications. PhD thesis, Johannes Gutenberg-Universität Mainz (2012)

[7] Manna, K., Sun, Y., Muechler, L., Kübler, J., Felser, C.: Heusler, weyl and berry. Nature Reviews Materials **3**(8) (2018) 244–256

[8] Wang, X.L., Dou, S.X., Zhang, C.: Zero-gap materials for future spintronics, electronics and optics. NPG asia materials **2**(1) (2010) 31–38

[9] Du, Y., Xu, G., Zhang, X., Liu, Z., Yu, S., Liu, E., Wang, W., Wu, G.: Crossover of magnetoresistance in the zero-gap half-metallic heusler alloy fe2cosi. EPL (Europhysics Letters) **103**(3) (2013) 37011

[10] Skaftouros, S., Özdoğan, K., Şaşıoğlu, E., Galanakis, I.: Generalized slater-pauling rule for the inverse heusler compounds. Physical Review B **87**(2) (2013) 024420

[11] Tuzcuoglu, H.: Corrélation entre les propriétés structurales et magnétiques des couches minces et nanostructures de CoFeAl. PhD thesis, Université Paris-Nord-Paris XIII (2014)

[12] Galanakis, I.: Theory of Heusler and Full-Heusler Compounds. In Felser, C., Hirohata, A., eds.: Heusler Alloys. Volume 222. Springer International Publishing, Cham (2016) 3–36 Series Title: Springer Series in Materials Science.

[13] Mattsson, A.E., Schultz, P.A., Desjarlais, M.P., Mattsson, T.R., Leung, K.: Designing meaningful density functional theory calculations in materials science—a primer. Modelling and Simulation in Materials Science and Engineering **13**(1) (2004) R1

[14] Weinberger, C.R., Tucker, G.J.: Multiscale materials modeling for nanomechanics. (2016)

[15] Woods, N.: On the nature of self-consistency in density functional theory. arXiv preprint arXiv:1803.01763 (2018)

[16] Kebede, A., Amde, A., Diaz, W.: Proceedings of the 4th gondar school of science and technology, 3 – 5 january 2014, university of gondar. (01 2014)

[17] Kirklin, S., Saal, J.E., Meredig, B., Thompson, A., Doak, J.W., Aykol, M., Rühl, S., Wolverton, C.: The open quantum materials database (oqmd): assessing the accuracy of dft formation energies. npj Computational Materials **1**(1) (2015) 1–15

[18] Felser, C., Fecher, G.H., eds.: Spintronics. Springer Netherlands, Dordrecht (2013)

[19] Chen, W., Buyanova, I.: Handbook of Spintronic Semiconductors. CRC Press (2019)

[20] Blügel, S., Waser, R., Bürgler, D., Schneider, C.M., Morgenstern, M.: Spintronics-from GMR to quantum information. Number PreJuSER-136125. Institut für Festkörperforschung (2009)

[21] Willoughby, A., Capper, P., Kasap, S.: Spintronics for next generation innovative devices. John Wiley & Sons (2015)

[22] Alloul, H.: Introduction to the Physics of Electrons in Solids. Springer Science & Business Media (2010)

[23] Hirohata, A., Takanashi, K.: Future perspectives for spintronic devices. Journal of Physics D: Applied Physics **47**(19) (2014) 193001

[24] Coey, J., Sanvito, o.S.: Magnetic semiconductors and half-metals. Journal of Physics D: Applied Physics **37**(7) (2004) 988

[25] Wang, X., Cheng, Z., Liu, G., Dai, X., Khenata, R., Wang, L., Bouhemadou, A.: Rare earth-based quaternary heusler compounds mcovz (m= lu, y; z= si, ge) with tunable band characteristics for potential spintronic applications. IUCrJ **4**(6) (2017) 758–768

[26] Faid, F., Elchikh, M., Bahlouli, S., Kaddar, K.: Strong correlation effect in ferrimagnetic half-metallic v 2 coal and v 2 coga heusler compounds. Journal of Superconductivity and Novel Magnetism **31**(8) (2018) 2491–2500

[27] De Groot, R., Mueller, F., Van Engen, P., Buschow, K.: New class of materials: half-metallic ferromagnets. Physical Review Letters **50**(25) (1983) 2024

[28] W. H. Wang, G. H. Wu, a.J.L.C.S.X.G., Zhan, W.S.: Intermartensitic transformation and magnetic-field-induced strain in ni52mn24.5ga23.5 single crystals. APPLIED PHYSICS LETTERS **79**(8) (20 AUGUST 2001) 1149

[29] Wen, G.H., Zhang, X.X.: New ferromacnelic heusler alloys. Journal of Physics D: Applied Physics (2003) 2

[30] Zongbin Chen, Huan Wei, H.X.Y.G.T.Y.X.W., Chen, X.: First-principles study on a new all-d-metal full-heusler-based shape-memory alloy cd2mnpd. UNIVERSITY OF NEW ENGLAND on 09/26/19 **9**(3) (13 June 2019) 1950012

[31] Hirohata, A., Yamada, K., Nakatani, Y., Prejbeanu, I.L., Diény, B., Pirro, P., Hillebrands, B.: Review on spintronics: Principles and device applications. Journal of Magnetism and Magnetic Materials **509** (2020) 166711

[32] Chen, X.Q., Podloucky, R., Rogl, P.: Ab initio prediction of half-metallic properties for the ferromagnetic heusler alloys co 2 m si (m= ti, v, cr). Journal of applied physics **100**(11) (2006) 113901

[33] Segall, M., Lindan, P.J., Probert, M.a., Pickard, C.J., Hasnip, P.J., Clark, S., Payne, M.: First-principles simulation: ideas, illustrations and the castep code. Journal of physics: condensed matter **14**(11) (2002) 2717

[34] Pozhar, L.: Virtual Synthesis of Nanosystems by Design: From First Principles to Applications. Elsevier (2015)

[35] Cerveró, J.M., Polo, P.P.: The one dimensional schrödinger equation: symmetries, solutions and feynman propagators. European Journal of Physics **37**(5) (2016) 055401

[36] Hladik, J., Chrysos, M., Hladik, P.E., Ancarani, L.U.: Mécanique quantique. Masson (1997)

[37] Hanaor, D.A., Assadi, M.H., Li, S., Yu, A., Sorrell, C.C.: Ab initio study of phase stability in doped tio 2. Computational Mechanics **50**(2) (2012) 185–194

[38] Rai, D.P., Sandeep, Shankar, A., Sakhya, A.P., Sinha, T.P., Khenata, R., Ghimire, M.P., Thapa, R.K.: Electronic and magnetic properties of X_2 YZ and XYZ Heusler compounds: a comparative study of density functional theory with different exchange-correlation potentials. Materials Research Express **3**(7) (July 2016) 075022

[39] Blügel, S., Jülich, K., eds.: Spintronics: from GMR to quantum information ; lecture notes of the 40th Spring School 2009. Number 10 in Schriften des Forschungszentrums Jülich Reihe Schlüsseltechnologien. Forschungszentrum, Zentralbibliothek, Jülich (2009) Meeting Name: Spring School. Institute of Solid State Research in the Research Centre JülichOCLC: 427648894.

[40] O'handley, R.C.: Soft magnetic materials. Modern Magnetic Materials **46** (2000)

[41] : 29. 7. 20031 III–5 Magnetic Properties of Materials - [PPT Powerpoint] (2003)

[42] Krishnan, K.M.: Magnetism on a microscopic scale. MRS Bulletin **20**(10) (1995) 24–28

[43] De Lacheisserie, E.d.T., Gignoux, D., Schlenker, M.: Magnetism. Volume 1. Springer Science & Business Media (2005)

[44] Issaoui, F.: Etude des propriétés magnétiques des matériaux à bases des métaux de transition sous forme de poudre (AúBO) et monocristaux (RMX). PhD thesis, Grenoble (2012)

[45] Sinn, E.: MAGNETIC PROPERTIES. (January 2005) 323–336

[46] Caraballo-Vivas, R.J.: Magnetism from intermetallics and perovskite oxides. arXiv preprint arXiv:1707.09868 (2017)

[47] Moskowitz, B.M.: Hitchhiker's guide to magnetism. In: Environmental Magnetism Workshop (IRM). Volume 279., Inst. for Rock Magnetism Univ. of Minn., Minneapolis, Minn (1991) 48

[48] Billah, A.: Investigation of multiferroic and photocatalytic properties of Li doped BiFeO3 nanoparticles prepared by ultrasonication. (2016) Publisher: Unpublished.

[49] Georges, P.: Introduction à l'étude du magnétisme. Université de Paris. École Supérieur d'Électricité (1966)

[50] Barbara, M.B.: Elaboration et Caractérisations Physiques des Manganites à Effet Magnétocalorique. 174

[51] Bihlmayer, G.: Density-functional Theory of Magnetism. In Kronmüller, H., Parkin, S., eds.: Handbook of Magnetism and Advanced Magnetic Materials. John Wiley & Sons, Ltd, Chichester, UK (December 2007) hmm101

[52] Kübler, J., Williams, A.: Itinerant theory of localized magnetism. Journal of Magnetism and Magnetic Materials **54-57** (February 1986) 603–606

[53] Lim, J.A.: The role of local versus itinerant magnetism: studies of dilute magnetic semiconductors and multi-k magnets. PhD thesis, University of Birmingham (2013)

[54] Mena, F.P.: Optics and magnetism: from itinerant to localized electrons. PhD thesis, s.n.], S.l. (2004) ISBN: 9789036721288 OCLC: 66574601.

[55] Coey, J.M.: Magnetism and magnetic materials. Cambridge university press (2010)

[56] Cullity, B.D., Graham, C.D.: Introduction to magnetic materials. John Wiley & Sons (2011)

[57] Buschow, K.H.J., Boer, F.R., et al.: Physics of magnetism and magnetic materials. Volume 7. (2003)

[58] Garad, H.M.: L'anisotropie magnétique perpendiculaire induite par oxydation et recuit thermique: De la structure au magnétisme. PhD thesis, Université de Grenoble (2012)

[59] Gupta, H.K., ed.: Encyclopedia of Solid Earth Geophysics. Encyclopedia of Earth Sciences Series. Springer Netherlands, Dordrecht (2011)

[60] Guechi, N.: Élaboration et caractérisations structurale, électrique et magnétique des couches minces de FexNi100-x déposées sur Si (100). PhD thesis (2018)

[61] Fert, A., Van Dau, F.N.: Spintronics, from giant magnetoresistance to magnetic skyrmions and topological insulators. Comptes Rendus Physique **20**(7-8) (2019) 817–831

[62] Pippard, A.B.: Magnetoresistance in metals. Volume 2. Cambridge university press (1989)

[63] McGuire, T., Potter, R.: Anisotropic magnetoresistance in ferromagnetic 3d alloys. IEEE Transactions on Magnetics **11**(4) (1975) 1018–1038

[64] Wu, H.: Structural and magnetic characterisation of Heusler alloy thin films under optimised growth condition for spintronic devices. PhD thesis, University of York (2018)

[65] Tang, D.D., Pai, C.F.: MAGNETIC MEMORY TECHNOLOGY: Spin-transfer-torque Mram and Beyond. John Wiley & Sons (2020)

[66] Liu, P., Lin, X., Xu, Y., Zhang, B., Si, Z., Cao, K., Wei, J., Zhao, W.: Optically tunable magnetoresistance effect: From mechanism to novel device application. Materials **11**(1) (2018) 47

[67] Rao, C., Raychaudhuri, A.: Colossal magnetoresistance, charge ordering and other novel properties of manganates and related materials. In: Advances In Chemistry: A Selection of CNR Rao's Publications (1994–2003). World Scientific (2003) 133–174

[68] Felser, C., Fecher, G.H., Balke, B.: Spintronics: a challenge for materials science and solid-state chemistry. Angewandte Chemie International Edition **46**(5) (2007) 668–699

[69] Camley, R.E., Barnaś, J.: Theory of giant magnetoresistance effects in magnetic layered structures with antiferromagnetic coupling. Physical review letters **63**(6) (1989) 664

[70] Grünberg, P., Schreiber, R., Pang, Y., Brodsky, M., Sowers, H.: Layered magnetic structures: Evidence for antiferromagnetic coupling of fe layers across cr interlayers. Physical review letters **57**(19) (1986) 2442

[71] Dieny, B., Goldfarb, R.B., Lee, K.J.: Introduction to magnetic random-access memory. John Wiley & Sons (2016)

[72] Fert, A., Van Dau, F.N.: Spintronics, from giant magnetoresistance to magnetic skyrmions and topological insulators. Comptes Rendus Physique **20**(7-8) (November 2019) 817–831

[73] Maekawa, S., ed.: Concepts in spin electronics. Number 13 in Series on semiconductor science and technology. Oxford University Press, Oxford ; New York (2006)

[74] Chatterjee, J.: Engineering of magnetic tunnel junction stacks for improved STT-MRAM performance and development of novel and cost-effective nano-patterning techniques. PhD thesis, Université Grenoble Alpes (2018)

[75] Wurmehl, S., Wójcik, M.: Structural order in heusler compounds. Heusler Alloys (2016) 87–109

[76] Kreiner, G., Kalache, A., Hausdorf, S., Alijani, V., Qian, J.F., Shan, G., Burkhardt, U., Ouardi, S., Felser, C.: New mn2-based heusler compounds. Zeitschrift für anorganische und allgemeine Chemie **640**(5) (2014) 738–752

[77] Meinert, M., Schmalhorst, J.M., Reiss, G.: Exchange interactions and curie temperatures of mn2coz compounds. Journal of Physics: Condensed Matter **23**(11) (2011) 116005

[78] Felser, C., Hirohata, A.: Heusler alloys. Springer (2015)

[79] Katsnelson, M., Irkhin, V.Y., Chioncel, L., Lichtenstein, A., de Groot, R.A.: Half-metallic ferromagnets: From band structure to many-body effects. Reviews of Modern Physics **80**(2) (2008) 315

[80] Bainsla, L., Suresh, K.: Equiatomic quaternary heusler alloys: A material perspective for spintronic applications. Applied Physics Reviews **3**(3) (2016) 031101

[81] Groom, C.R., Allen, F.H.: The cambridge structural database in retrospect and prospect. Angewandte Chemie International Edition **53**(3) (2014) 662–671

[82] Alijani, V., Winterlik, J., Fecher, G.H., Naghavi, S.S., Felser, C.: Quaternary half-metallic heusler ferromagnets for spintronics applications. Physical Review B **83**(18) (2011) 184428

[83] Galanakis, I., Özdoğan, K., Şaşıoğlu, E.: Spin-filter and spin-gapless semiconductors: The case of heusler compounds. AIP Advances **6**(5) (2016) 055606

[84] Fichtner, T.: Synthesis and characterization of mn-rich heusler alloys for magnetocaloric applications. (2016)

[85] De Groot, R., Buschow, K.: Recent developments in half-metallic magnetism. Journal of Magnetism and Magnetic Materials **54** (1986) 1377–1380

[86] Kübler, J., William, A., Sommers, C.: Formation and coupling of magnetic moments in heusler alloys. Physical Review B **28**(4) (1983) 1745

[87] Alijani, V., Winterlik, J., Fecher, G.H., Felser, C.: Tuning the magnetism of the heusler alloys mn3- x co x ga from soft and half-metallic to hard-magnetic for spin-transfer torque applications. Applied Physics Letters **99**(22) (2011) 222510

[88] Kandpal, H.C., Fecher, G.H., Felser, C.: Calculated electronic and magnetic properties of the half-metallic, transition metal based heusler compounds. Journal of Physics D: Applied Physics **40**(6) (2007) 1507

[89] Ouardi, S., Fecher, G.H., Felser, C., Kübler, J.: Realization of spin gapless semiconductors: The heusler compound mn 2 coal. Physical review letters **110**(10) (2013) 100401

[90] Wang, X.: Proposal for a new class of materials: spin gapless semiconductors. Physical review letters **100**(15) (2008) 156404

[91] Yue, Z., Li, Z., Sang, L., Wang, X.: Spin-gapless semiconductors. Small **16**(31) (2020) 1905155

[92] Huang, H., Yang, K., Zhao, W., Zhou, T., Yang, X., Wu, B.: High-pressure-induced transition from ferromagnetic semiconductor to spin gapless semiconductor in quaternary heusler alloy vfescz (z= sb, as, p). Applied Sciences **9**(14) (2019) 2859

[93] Wang, X., Cheng, Z., Wang, J., Wang, X.L., Liu, G.: Recent advances in the heusler based spin-gapless semiconductors. Journal of Materials Chemistry C **4**(30) (2016) 7176–7192

[94] Xu, G., Liu, E., Du, Y., Li, G., Liu, G., Wang, W., Wu, G.: A new spin gapless semiconductors family: Quaternary heusler compounds. EPL (Europhysics Letters) **102**(1) (2013) 17007

[95] Ma, J., Hegde, V.I., Munira, K., Xie, Y., Keshavarz, S., Mildebrath, D.T., Wolverton, C., Ghosh, A.W., Butler, W.: Computational investigation of half-heusler compounds for spintronics applications. Physical Review B **95**(2) (2017) 024411

[96] Gao, G., Yao, K.L.: Antiferromagnetic half-metals, gapless half-metals, and spin gapless semiconductors: The d03-type heusler alloys. Applied Physics Letters **103**(23) (2013) 232409

[97] Bainsla, L., Mallick, A., Raja, M.M., Coelho, A., Nigam, A., Johnson, D., Alam, A., Suresh, K.: A new spin gapless semiconductor: quaternary heusler cofecrga alloy. arXiv preprint arXiv:1411.5772 (2014)

[98] Rani, D., Bainsla, L., Alam, A., Suresh, K.: Spin-gapless semiconductors: Fundamental and applied aspects. Journal of Applied Physics **128**(22) (2020) 220902

[99]

[100] Carey, F.A., Sundberg, R.J.: Chemical bonding and molecular structure. In: Advanced Organic Chemistry. Springer (2007) 1–117

[101] Jain, V.K.: The concept of hybridization : A rapid and new innovative method for prediction of hybridized state of an atom in a very short time. Indian Journal of Applied Research 55 **14**(7) (2014) 1–4

[102] Bezverkhniy, V., Bezverkhniy, V.: Hybridization theory of l. pauling, chemical bond and quantum mechanics. Pauling, Chemical Bond and Quantum Mechanics (February 24, 2019) (2019)

[103] Khomskii, D.I., Streltsov, S.V.: Orbital effects in solids: Basics, recent progress, and opportunities. Chemical Reviews **121**(5) (2020) 2992–3030

[104] Landron, S., Lepetit, M.B.: Importance of t 2 g- e g hybridization in transition metal oxides. Physical Review B **77**(12) (2008) 125106

[105] Bhattacharjee, S., Lee, S.S., Kim, Y.B.: Spin–orbital locking, emergent pseudo-spin and magnetic order in honeycomb lattice iridates. New Journal of Physics **14**(7) (2012) 073015

[106] Chen, Z., Liu, W., Chen, P., Ruan, X., Sun, J., Liu, R., Gao, C., Du, J., Liu, B., Meng, H., et al.: Direct observation of ferrimagnetic ordering in inverse heusler alloy mn2coal. Applied Physics Letters **117**(1) (2020) 012401

[107] Burns, R.G., Burns, R.G.: Mineralogical applications of crystal field theory. Number 5. Cambridge university press (1993)

[108] Nawa, K., Miura, Y.: Exploring half-metallic co-based full heusler alloys using a dft+ u method combined with linear response approach. RSC advances **9**(52) (2019) 30462–30478

[109] Slater, J.C.: The ferromagnetism of nickel. Physical Review **49**(7) (1936) 537

[110] Pauling, L.: The nature of the interatomic forces in metals. Physical Review **54**(11) (1938) 899

[111] Fecher, G.H., Kandpal, H.C., Wurmehl, S., Felser, C., Schönhense, G.: Slater-pauling rule and curie temperature of co 2-based heusler compounds. Journal of applied physics **99**(8) (2006) 08J106

[112] Luo, H., Meng, F., Liu, H., Li, J., Liu, E., Wu, G., Zhu, X., Jiang, C.: Origin of the z- 28 rule in mn2cu-based heusler alloys: A comparing study. Journal of magnetism and magnetic materials **324**(13) (2012) 2127–2130

[113] Luo, H., Liu, G., Meng, F., Wang, L., Liu, E., Wu, G., Zhu, X., Jiang, C.: Slater–pauling behavior and half-metallicity in heusler alloys mn2cuz (z= ge and sb). Computational materials science **50**(11) (2011) 3119–3122

[114] Schrödinger, E.: An undulatory theory of the mechanics of atoms and molecules. Physical review **28**(6) (1926) 1049

[115] Sholl, D., Steckel, J.A.: Density functional theory: a practical introduction. John Wiley & Sons (2011)

[116] Gross, E.K., Dreizler, R.M.: Density functional theory. Volume 337. Springer Science & Business Media (2013)

[117] Tsuneda, T.: Density functional theory in quantum chemistry. (2014)

[118] Giustino, F.: Materials modelling using density functional theory: properties and predictions. Oxford University Press (2014)

[119] Joubert, D.: Density functionals: theory and applications. Volume 500. (1998)

[120] Dreizler, R.M., Gross, E.K.: Density functional theory: an approach to the quantum many-body problem. Springer Science & Business Media (2012)

[121] Schrödinger, E.: An undulatory theory of the mechanics of atoms and molecules. Phys. Rev. **28** (Dec 1926) 1049–1070

[122] Schrödinger, E.: Mémoires sur la mécanique ondulatoire. Bull. Amer. Math. Soc **39** (1933) 854

[123] Born, M., Oppenheimer, J.R.: On the quantum theory of molecules. (1927)

[124] Cohen, C., Tannoudji, B.D., Laloë, F.: Mécanique quantique. Vol. I–II, Collection Enseignement des sciences **16** (1973)

[125] Sherrill, C.D.: The born-oppenheimer approximation. School of Chemistry and Biochemistry, Georgia Institute of Technology **242** (2005)

[126] Baer, M.: Beyond Born-Oppenheimer: termes de couplage électronique non adiabatique et intersections coniques. (2006)

[127] Thomas, L.H.: The calculation of atomic fields. In: Mathematical proceedings of the Cambridge philosophical society. Volume 23., Cambridge University Press (1927) 542–548

[128] Lieb, E.H.: A brief review of thomas-fermi theory. Departments of Physics and Mathematics, Jadwin Hall, Princeton University, PO Box **708** (2000)

[129] Kohn, W., Sham, L.J.: Self-consistent equations including exchange and correlation effects. Physical review **140**(4A) (1965) A1133

[130] Gervat, A.: Quelques propriétés de la matière à des températures très htgh et à des pressions élevées (équations d'état, opacité); quelques propriétaires de la matière aux tres hautes températures et fortes presses (équation d'état, opacite). (1964)

[131] Hohenberg, P., Kohn, W.: Inhomogeneous electron gas. Phys. Rev. **136** (Nov 1964) B864–B871

[132] Ranaivoson, R., Raoelina, A., Andrianiaina, H., Hanitriarivo, R.: Density functional theory and its applications in nanotechnology. (2018)

[133] Hohenberg, P., Kohn, W.: Inhomogene electron gas. Physical review **136**(3B) (1964) B864

[134] Parr, R., Yang, W.: Density-functional theory of the electronic structure of molecules. Annual Review of Physical Chemistry **46** (1995) 701 –728

[135] Weso l owski, T.A.: Hohenberg-kohn-sham density functionory thory. In: Molecular Materials with Specific Interactions - Modeling. 153 –201

[136] Freyss, M.: Density functional theory. Technical report (2015)

[137] Sham, L.J., Kohn, W.: One-particle properties of an inhomogeneous interacting electron gas. Physical Review **145**(2) (1966) 561

[138] Frayret, C.: Application de la Théorie de la Fonctionnelle de la Densité à la modélisation de la diffusion de l'ion oxygène dans des électrolytes solides modèles et des conducteurs mixtes. PhD thesis, Université Sciences et Technologies-Bordeaux I (2004)

[139] Perdew, J.P., Wang, Y.: Accurate and simple analytic representation of the electron-gas correlation energy. Physical review B **45**(23) (1992) 13244

[140] Jones, R.O., Gunnarsson, O.: The density functional formalism, its applications and prospects. Reviews of Modern Physics **61**(3) (1989) 689

[141] Dirac, P.A.: Note on exchange phenomena in the thomas atom. In: Mathematical proceedings of the Cambridge philosophical society. Volume 26., Cambridge University Press (1930) 376–385

[142] Perdew, J.P., Burke, K., Ernzerhof, M.: Generalized gradient approximation made simple. Physical review letters **77**(18) (1996) 3865

[143] Perdew, J.P., Ruzsinszky, A., Csonka, G.I., Vydrov, O.A., Scuseria, G.E., Constantin, L.A., Zhou, X., Burke, K.: Restoring the density-gradient expansion for exchange in solids and surfaces. Physical review letters **100**(13) (2008) 136406

[144] Pedroza, L.S., da Silva, A.J., Capelle, K.: Gradient-dependent density functionals of the perdew-burke-ernzerhof type for atoms, molecules, and solids. Physical Review B **79**(20) (2009) 201106

[145] Terentjev, A.V., Constantin, L.A., Pitarke, J.M.: Dispersion-corrected pbesol exchange-correlation functional. Physical review B **98**(21) (2018) 214108

[146] Perdew, J.P., Kurth, S.: Density functionals for non-relativistic coulomb systems in the new century. In: A primer in density functional theory. Springer (2003) 1–55

[147] Ashcroft, N.W., Mermin, N.D., et al.: Solid state physics (1976)

[148] Korringa, J.: On the calculation of the energy of a bloch wave in a metal. Physica **13**(6-7) (1947) 392–400

[149] Kresse, G., Furthmüller, J.: Efficient iterative schemes for ab initio total-energy calculations using a plane-wave basis set. Physical review B **54**(16) (1996) 11169

[150] Monkhorst, H.J., Pack, J.D.: Special points for brillouin-zone integrations. Physical review B **13**(12) (1976) 5188

[151] Chadi, D., Cohen, M.L.: Special points in the brillouin zone. Physical Review B **8** (1973) 5747–5753

[152] Joannopoulos, J.D., Cohen, M.L.: Electronic charge densities for zns in the wurtzite and zincblende structures. Journal of Physics C: Solid State Physics **6**(9) (1973) 1572

[153] Evarestov, R., Smirnov, V.: Special points of the brillouin zone and their use in the solid state theory. Physica Status Solidi B-basic Solid State Physics **119** (1983) 9–40

[154] Jochym, D.B.: Development of non-local density functional methods. PhD thesis, Durham University (2008)

[155] Payne, M.C., Teter, M.P., Allan, D.C., Arias, T., Joannopoulos, a.J.: Iterative minimization techniques for ab initio total-energy calculations: molecular dynamics and conjugate gradients. Reviews of modern physics **64**(4) (1992) 1045

[156] Filippetti, A., Bachelet, G.: Pseudopotential method. (2005)

[157] Martin, R.M.: Electronic structure: basic theory and practical methods. Cambridge university press (2020)

[158] Richard, N.: Actinides and lanthanides under pressure: the pseudopotential approach; actinides et terres rares sous pression: approche pseudopotentiel. (2002)

[159] Sommerfeld, A.: Zur Elektronentheorie der Metalle auf Grund der Fermischen Statistik. Zeitschrift für Physik **47**(1) (January 1928) 1–32

[160] Fermi, E.: Sopra lo Spostamento per Pressione delle Righe Elevate delle Serie Spettrali. Il Nuovo Cimento (1924-1942) **11**(3) (September 2008) 157

[161] Hellmann, H.: A new approximation method in the problem of many electrons. The Journal of Chemical Physics **3**(1) (1935) 61–61

[162] Tran, R.: The empirical pseudopotential method

[163] Hogan, S., Merkt, F.: A new perspective on the binding power of an electron. ChemPhysChem **10**(17) (2009) 2931–2934

[164] Phillips, J.C., Kleinman, L.: New method for calculating wave functions in crystals and molecules. Phys. Rev. **116** (Oct 1959) 287–294

[165] Antončík, E.: Approximate formulation of the orthogonalized plane-wave method. Journal of Physics and Chemistry of solids **10**(4) (1959) 314–320

[166] Laasonen, K., Pasquarello, A., Car, R., Lee, C., Vanderbilt, D.: Car-parrinello molecular dynamics with vanderbilt ultrasoft pseudopotentials. Physical Review B **47**(16) (1993) 10142

[167] Smallwood, C.J., Larsen, R.E., Glover, W.J., Schwartz, B.J.: A computationally efficient exact pseudopotential method. i. analytic reformulation of the phillips-kleinman theory. The Journal of chemical physics **125**(7) (2006) 074102

[168] Hamann, D.R., Schlüter, M., Chiang, C.: Norm-conserving pseudopotentials. Phys. Rev. Lett. **43** (Nov 1979) 1494–1497

[169] Zeffane, S., Sayah, M., Dahmane, F., Mokhtari, M., Zekri, L., Khenata, R., Zekri, N.: Prediction of electronic and half metallic properties of mn _2 ysn (y= mo, nb, zr) heusler alloys. arXiv preprint arXiv:2103.15542 (2021)

[170] Aryal, A., Bakkar, S., Samassekou, H., Pandey, S., Dubenko, I., Stadler, S., Ali, N., Mazumdar, D.: Mn2FeSi: An antiferromagnetic inverse-Heusler alloy. Journal of Alloys and Compounds **823** (May 2020) 153770

[171] Grimme, S.: Semiempirical gga-type density functional constructed with a long-range dispersion correction. Journal of computational chemistry **27**(15) (2006) 1787–1799

[172] De La Pierre, M., Orlando, R., Maschio, L., Doll, K., Ugliengo, P., Dovesi, R.: Performance of six functionals (lda, pbe, pbesol, b3lyp, pbe0, and wc1lyp) in the simulation of vibrational and dielectric properties of crystalline compounds. the case of forsterite mg2sio4. Journal of computational chemistry **32**(9) (2011) 1775–1784

[173] Jacobsen, E., Lyons, R.: The sliding dft. IEEE Signal Processing Magazine **20**(2) (2003) 74–80

[174] Pauling, L., Brockway, L.: The crystal structure of chalcopyrite cufes2. Zeitschrift für Kristallographie-Crystalline Materials **82**(1-6) (1932) 188–194

[175] Dai, Y.H.: Convergence properties of the bfgs algoritm. SIAM Journal on Optimization **13**(3) (2002) 693–701

[176] Yang, T., Cao, J., Wang, X.: Structural, electronic, magnetic, mechanic and thermodynamic properties of the inverse heusler alloy ti2niin under pressure. Crystals **8**(11) (2018) 429

[177] Saal, J.E., Kirklin, S., Aykol, M., Meredig, B., Wolverton, C.: Materials design and discovery with high-throughput density functional theory: the open quantum materials database (oqmd). Jom **65**(11) (2013) 1501–1509

[178] Mokhtari, D.J., Jum'h, I., Baaziz, H., Charifi, Z., Ghellab, T., Telfah, A., Hergenröder, R.: Structural, electronic, magnetic and thermoelectric properties of inverse Heusler alloys Ti $_2$ CoSi, Mn $_2$ CoAl and Cr $_2$ ZnSi by employing Ab initio calculations. Philosophical Magazine **100**(12) (June 2020) 1636–1661

[179] Birch, F.: Finite elastic strain of cubic crystals. Physical review **71**(11) (1947) 809

[180] Tyuterev, V., Vast, N.: Murnaghan's equation of state for the electronic ground state energy. Computational materials science **38**(2) (2006) 350–353

[181] Nave, R.: Bulk elastic properties. HyperPhysics. Georgia State University (2016)

[182] Gallas, M.R., Piermarini, G.J.: Bulk modulus and young's modulus of nanocrystalline γ-alumina. Journal of the American Ceramic Society **77**(11) (1994) 2917–2920

[183] Willert, E., Forsbach, F., Popov, V.L.: Stress tensor and gradient of hydrostatic pressure in the contact plane of axisymmetric bodies under normal and tangential loading (2020)

[184] Nihous, G.C.: Notes on hydrostatic pressure. Journal of Ocean Engineering and Marine Energy **2**(1) (2016) 105–109

[185] Zou, P., Bader, R.: A topological definition of a wigner–seitz cell and the atomic scattering factor. Acta Crystallographica Section A: Foundations of Crystallography **50**(6) (1994) 714–725

[186] Misra, P.: Physics of condensed matter. Academic Press (2011)

[187] Setyawan, W., Curtarolo, S.: High-throughput electronic band structure calculations: Challenges and tools. Computational materials science **49**(2) (2010) 299–312

[188] Piela, L.: Ideas of quantum chemistry. Elsevier (2006)

[189] Misra, P.K.: Chapter 4 - nearly free electron model. In Misra, P.K., ed.: Physics of Condensed Matter. Academic Press, Boston (2012) 95–130

[190] Sham, L.J., Schlüter, M.: Density-functional theory of the energy gap. Physical Review Letters **51**(20) (1983) 1888

[191] Trügler, A.: Optical properties of metallic nanoparticles: basic principles and simulation. Volume 232. Springer (2016)

[192] Lamontagne, L.K.: Band structures and the meaning of the wave vector k

[193] Mohamed, M.M.: Etude ab-initio des propriétés physiques des matériaux Heusler (X2YZ) et demi Heusler (XYZ). PhD thesis, Université de Mascara (2020)

[194] Mead, C., Spitzer, W.: Fermi level position at metal-semiconductor interfaces. Physical Review **134**(3A) (1964) A713

[195] Kittel, C., McEuen, P., McEuen, P.: Introduction to solid state physics. Volume 8. Wiley New York (1996)

[196] Dufek, P., Blaha, P., Schwarz, K.: Applications of engel and vosko's generalized gradient approximation in solids. Physical Review B **50**(11) (1994) 7279

[197] Engel, E., Vosko, S.H.: Exact exchange-only potentials and the virial relation as microscopic criteria for generalized gradient approximations. Physical Review B **47**(20) (1993) 13164

[198] FAID, F.: Contribution à l'étude des alliages Heusler à base de Vanadium par les méthodes de premier principe. PhD thesis, Université Mohamed Boudiaf des Sciences et de la Technologie-Mohamed Boudiaf ...

[199] Mulliken, R.S.: Electronic population analysis on lcao–mo molecular wave functions. i. The Journal of Chemical Physics **23**(10) (1955) 1833–1840

[200] Faleev, S.V., Ferrante, Y., Jeong, J., Samant, M.G., Jones, B., Parkin, S.S.: Origin of the tetragonal ground state of heusler compounds. Physical Review Applied **7**(3) (2017) 034022

[201] Saha, S., Roy, R.K., Ayers, P.W.: Are the hirshfeld and mulliken population analysis schemes consistent with chemical intuition? International journal of quantum chemistry **109**(9) (2009) 1790–1806

[202] Brown, P., Bargawi, A.Y., Crangle, J., Neumann, K.U., Ziebeck, K.: Direct observation of a band jahn-teller effect in the martensitic phase transition of ni2mnga. Journal of Physics: Condensed Matter **11**(24) (1999) 4715

[203] Pavarini, E.: Crystal-field theory, tight-binding method and jahn-teller effect. Correlated electrons: from models to materials **2** (2012) 6–2

[204] Muthui, Z., Musembi, R., Mwabora, J., Kashyap, A.: Effect of the y element on the structural, electronic and magnetic properties of heusler compounds co2yin (y= v, nb, and ti): An ab initio study. AIP Advances **11**(1) (2021) 015107

[205] Liu, D.C., Nocedal, J.: On the limited memory bfgs method for large scale optimization. Mathematical programming **45**(1) (1989) 503–528

[206] Fletcher, R.: Practical methods of optimization. (1988)

[207] Hasnip, P.: Bands-parallelism in castep a dcse project. (2008)

[208] Clark, S.J., Segall, M.D., Pickard, C.J., Hasnip, P.J., Probert, M.I., Refson, K., Payne, M.C.: First principles methods using castep. Zeitschrift für Kristallographie-Crystalline Materials **220**(5-6) (2005) 567–570

[209] Agarwal, P.K., Sharir, M.: Efficient algorithms for geometric optimization. ACM Computing Surveys (CSUR) **30**(4) (1998) 412–458

[210] Tsompanakis, Y., Lagaros, N.D., Papadrakakis, M.: Innovative computational methods for shape optimization. In: 5th GRACM Congress on Computational Mechanics. (2002)

[211] Jappor, H.R., Abdulsattar, M.A., Abdul-Lettif, A.M.: Electronic structure of alp under pressure using semiempirical method. The Open Condensed Matter Physics Journal **3**(1) (2010)

[212] Kaxiras, E.: Atomic and electronic structure of solids. Cambridge University Press (2003)

[213] Chow, P., Liu, L.: Relativistic effects on the electronic band structure of compound semiconductors. Physical Review **140**(5A) (1965) A1817

[214] Bououdina, M.: Handbook of research on nanoscience, nanotechnology, and advanced materials. IGI Global (2014)

[215] Crépieux, A.: Introduction à la physique de la matière condensée: Propriétés électroniques. Dunod (2019)

[216] Bennett, L.H.: Electronic Density of States: Based on Invited and Contributed Papers and Discussion. Volume 323. US National Bureau of Standards (1971)

[217] Madelung, O.: Introduction to solid-state theory. Volume 2. Springer Science & Business Media (2012)

[218] Clark, A.E., Sonnenberg, J.L., Hay, P.J., Martin, R.L.: Density and wave function analysis of actinide complexes: What can fuzzy atom, atoms-in-molecules, mulliken, löwdin, and natural population analysis tell us? The Journal of chemical physics **121**(6) (2004) 2563–2570

[219] Sanchez-Portal, D., Artacho, E., Soler, J.M.: Projection of plane-wave calculations into atomic orbitals. Solid State Communications **95**(10) (1995) 685–690

[220] Martin, F., Zipse, H.: Charge distribution in the water molecule—a comparison of methods. Journal of computational chemistry **26**(1) (2005) 97–105

[221] Carbó-Dorca, R., Bultinck, P.: Quantum mechanical basis for mulliken population analysis. Journal of mathematical chemistry **36**(3) (2004) 231–239